UNIVERSITY OF TWENTE.

Faculty of Engineering Technology
Department of Biomechanical Engineering

Master Thesis

Evaluation of a Force Controlled Pneumatically Actuated Knee Orthosis

BE-831

Janine Klein Rot
s1367277

Graduation committee
Dr. E.H.F. van Asseldonk
Prof.dr.ir. H. van der Kooij
Dr.ir. B.J.F. van Beijnum

12-2021

Abstract

Exoskeletons are able to provide assistance to the wearer while walking. However, their rigid structure and weight limit the possibilities of these devices. Exosuits, soft wearable devices, provide tensile forces whereas exoskeletons provide compression forces. They are known to have lower weight and inertia compared to exoskeletons and could in the future be worn under clothing, due to the flexibility of the actuators. However, shear forces between the device and the body are larger in exosuits compared to exoskeletons, which causes the amount of force that can be delivered to be decreased. The inverted muscle skeleton approach inverts biology to provide assistance, instead of mimicking biology like exosuits. Less undesirable shear forces are present compared to exosuits, since compression forces instead of tension forces are delivered by the device. However, it has more rigid parts compared to exosuits and the inverted muscle skeleton approach could not be applied to all joints.

In this thesis, a pneumatically actuated knee orthosis, following the inverted muscle skeleton approach, is evaluated based on the performance of the force control mechanism, the performance of the assistive strategy, and the motion of the orthosis with respect to the body.

The orthosis consists of two cylinders mounted in parallel between two shells. The orthosis is attached to the wearer by placing the upper shell against the posterior side of the upper leg and the lower shell against the posterior side of the lower leg. The orthosis is kept in place with a structure of flexible attachments. The force control mechanism of the orthosis consists of a sliding mode controller, based on a mathematical model of the orthosis, and a controller proportional to the force tracking error. The orthosis can operate in minimal impedance mode and in assistive mode. In minimal impedance mode, the force the orthosis should deliver during walking is always 0 N. In assistive mode, an extension force should be delivered during the stance phase of the right leg, while during the swing phase, a force of 0 N should be delivered.

Five subjects participated in the experimental validation that started with a static trial. Thereafter, three walking trials on a treadmill were performed with the orthosis in minimal impedance mode and assistive mode. During the trials, the data from several sensors on the orthosis was recorded, together with muscle activity measurements of several muscles in the right leg. With a motion capture system, the movement of the shells and the upper and lower leg were recorded. The data was synchronized and thereafter processed in Matlab.

The force control mechanism performed well in terms of force tracking error. The force tracking error was smaller with the orthosis in minimal impedance mode compared to assistive mode. The assistive strategy performed well in terms of gait interference. The gait phase duration and the knee joint angle, the latter only during the swing phase, were not interfered by the provided assistance. The knee joint angle during the stance phase was interfered by the provided assistance, as the assistive strategy was designed to do. It could not be determined if the assistive strategy interfered with the muscle activity, since the measured activities did not correspond with literature. The orthosis moved with respect to the body in terms of relative displacement and relative rotation. Those movements were not equal for the upper and lower leg and shells. The maximum relative displacement, maximum relative rotation, and the relative displacement during the gait cycle were not interfered by the provided assistance. The relative rotation during the gait cycle was interfered by the provided assistance.

Contents

Chapter 1

Introduction

This chapter introduces the concept of exoskeletons, exosuits and the inverted muscle skeleton approach. It describes two main categories of force control mechanisms used in exoskeletons throughout literature. Thereafter, findings in literature on motion of assistive devices with respect to the body are described. Finally, the goal of this research is stated, followed by a plan of action to reach this goal.

1.1 Exoskeletons

The development of exoskeletons, active electromechanical devices worn by humans that match the shape and function of the body, began in the 1960s [1, 2]. Augmenting the ability of able-bodied subjects and providing assistance to impaired subjects, often as part of gait rehabilitation, are the main applications of exoskeletons [1, 2, 3]. In the latter case, which is the application of the device evaluated in this study, an exoskeleton can also be referred to as an active orthosis. [1].

In the past six decades, large steps were taken in the development of active orthoses. Early active orthoses were braces enhanced with a mechanism to provide assistance, such as the device described in [4] in which a spring is winded up. One of the first controllable active orthoses, described in [5], locks and unlocks the joints of the orthosis depending on the gait of the wearer. Later on, several active controllable orthoses were developed, powered by for example a dc motor, series elastic actuator, or pneumatic actuator, and controlled based on foot switches in the soles, muscle activity, ground reaction forces, or joint angles [6, 7, 8].

However, some challenges still remain in the field of active orthoses. First, the use of the active orthoses outside of experiments and therapy is limited by the portability of the actuators [1]. Second, the efficiency of the assistance relies on the rigid structure being perfectly aligned with the body [3]. As a result, it is harder to design an active orthosis that is applicable for a variety of subjects [1]. Third, the addition of rigid structures to the body could interfere with the biomechanics of the wearer and add extra weight to carry [3]. At last, related to the added weight, only a few active orthoses decrease the metabolic cost during several activities [1, 3].

1.2 Exosuits

Soft wearable devices called exosuits, designed to deliver assistive torques to biological joints, have a different approach in assisting the wearer compared to exoskeletons [9, 10]. The forces delivered by an exosuit are tensile forces, while exoskeletons can deliver torques and compression forces as well [3]. These tensile forces mimick the function of the muscles in the lower extremities [10]. Examples of mechanisms to deliver these tensile forces in exosuits are actuators connected to Bowden cables and pneumatic actuators that shorten when air is supplied [9, 10].

Exosuits have several advantages compared to exoskeletons. First, due to a lower weight and

inertia, it requires less metabolic cost to wear an exosuit compared to an exoskeleton [3, 10]. Second, the flexibility of the actuators could, in the future, allow for the exosuit to be worn under regular clothing [3, 10]. As a result, the wearer can blend in with society and use the full potential of protective clothing on top [3]. Due to its rigid structure, it is less likely that exoskeletons can be worn under regular clothing. Third, the kinematics of the wearer are less constrained by exosuits compared to exoskeletons, as they are composed of flexible materials around the body instead of rigid components [3, 10]. Related to this advantage, it is easier to adjust the exosuit to anatomical variations due to the flexibility of the device [3].
However, exosuits have some disadvantages compared to exoskeletons as well. First, forces delivered by the exosuit could result in movement of the exosuit with respect to the body [10]. As a result, shear forces are exerted on the body's surface and less force is destined to assist the wearer [10]. This effect is less prone in exoskeletons, due to the fact that in exoskeletons the body follows the movement of the device [10]. Related to this disadvantage, the maximum force an exosuit can exert on the human body is smaller compared to exoskeletons [3, 10]. Second, exosuits are unable to exert compressive loads, which exoskeletons are capable of [3].

1.3 Inverted muscle skeleton approach

Instead of mimicking biology, the approach used in exosuits, the inverted muscle skeleton (iMS) approach inverts biology to provide assistance [11]. By delivering compression instead of tension forces, the direction of shear forces on the body is inverted. A network of cables across biological joints is used to cancel out shear forces, or transform shear forces to compression forces on bony landmarks such as the hip [11].
The iMS approach has some advantages and disadvantages compared to exosuits and exoskeletons. First, a device based on the iMS approach can deliver higher assistive forces compared to an exosuit, due to the decrease in undesirable shear forces. However, there is still a limit on the maximum assistive force considering the comfort of the wearer. The shear forces that are not cancelled out are transformed into compression forces on other parts of the body, that could cause discomfort as well [12]. Second, the device based on the iMS approach can be lighter and less bulky compared to exoskeletons, but could have more rigid parts compared to exosuits [10]. Third, the principle is not applicable for all joints, while this is possible for both exosuits and exoskeletons [11].
In [11], a pneumatically actuated knee orthosis based on the iMS approach is designed and created, shown in Figure 2.1. It consists of two pneumatical cylinders, attached in parallel to a shell at each end. The shells of the orthosis are positioned at the posterior side of the upper and lower leg and are kept in place by means of a mesh of straps. The orthosis successfully delivered assistive torques to the knee joint during one-legged squats, which led to a decrease in muscle activity during extension [11].

1.4 Control of assistive device

Exoskeletons, exosuits, and assistive devices based on the iMS approach require a control mechanism to provide assistance to the wearer. To do so, it controls the human-device cooperation system that consists of the assistive device and the wearer, which are closely connected [13, 14]. Two main categories of control mechanisms have been successfully implemented in devices to assist the knee joint.
Trajectory tracking is a control mechanism, mainly used in gait rehabilitation, that replays desired joint trajectories, collected from healthy individuals, on the assistive device [13, 14, 15]. A drawback of this control mechanism is that it forces the wearer to walk according to the trajectory while not considering their initiatives for movements outside of this trajectory. It is therefore mainly used for humans with weak muscle strength or that have no or only partial

voluntary movements [13, 14].
In several studies, trajectory tracking has been successfully implemented. In [16], knee joint trajectories, obtained from literature, were adjusted and thereafter used as reference joint angle in a driven gait orthosis. The orthosis could provide the assistance to the wearer at least as effective as manual training by therapists and it allowed the walking speed to be higher compared to manual training. In [17], the reference knee joint angle for a powered knee orthosis depends on the knee joint angle and predefined normal gait, computed by measuring gait parameters from healthy humans. The device could provide a normal knee joint angle pattern and assist the wearer during walking.
The assist-as-needed control mechanism provides only the assistance the wearer needs to complete the task. [13, 14, 15]. This mechanism encourages the participation of the wearer, since it only provides assistance if the wearer needs it. It is therefore more suitable for humans that are able to provide some voluntary movements, compared to trajectory tracking.
In several studies, assist-as-needed control has been successfully implemented. In [18], an exoskeleton to support the knee was controlled by a set of different controllers. Which controller was active, was based on the action performed by the wearer. The algorithm for using the correct controllers at the correct moment in time was verified in an experimental validation. In [19], the Lokomat gait rehabilitation robot kept the knee joint angle within range of a desired trajectory by using compliant virtual walls. The control mechanism allowed the wearer to determine the timing of movements, while the desired trajectory was still adhered. The provided assistance decreased the muscle activity needed during walking.

1.5 Movement of assistive device with respect to body

Inefficient transfer of force exerted by an exoskeleton or exosuit is a critical problem in assistive devices. Up to 50% of the amount of assistance provided to the wearer could be absorbed [20, 21]. By gaining insight in the absorption of assistive forces, the performance of assistive devices may be improved [22].
For exoskeletons and exosuits, two ways for provided assistance to be absorbed have been found. First, the delivered force could result in deformation of the soft tissue underneath [22, 12]. Exoskeletons, which deliver assistive forces more orthogonally compared to exosuits, would compress, whereas exosuits would stretch the underlying soft tissue [22]. Second, misalignment of the device or stretching of its materials could result in changes in interaction forces between the device and the body and in movement of the device with respect to the body [10, 23].
Relative motion of an assistive device with respect to the body has been quantified in several studies. In [24], the movement of an active pelvis orthosis with respect to the body increased with increasing provided assistance. Increasing the walking speed increased the relative movement at the thigh. In [25], the knee and hip joint positions were different when comparing the joint positions of the Lokomat and the joint positions of the subject, which indicated relative motion. In [26], for a powered ankle foot orthosis with a customized physical interface, less relative motion was found between the body and the device, which was the purpose of the interface.

1.6 Goal

The purpose of this study is to evaluate the pneumatically actuated knee orthosis, designed in [11], during treadmill walking. The evaluation of the orthosis is based on three criteria. First, the performance of the force control mechanism in terms of the force tracking error. Second, the performance of the assistive strategy in terms of interference with gait and muscle activity. Third, the motion of the orthosis with respect to the body in terms of relative displacement and relative rotation.

To reach this goal, several steps were taken, which are described in this thesis. First, a force control mechanism was designed for the orthosis. To do so, a mathematical model of the orthosis was created. Second, an assistive strategy was designed to assist the wearer during walking. Third, an experimental validation was performed in which the subjects walked on a treadmill, while wearing the orthosis. The orthosis provided assistance in part of the trials, while in the other trials, the orthosis did not provide assistance to the wearer. Fourth, the data recorded during the experimental validation was processed and analyzed. Finally, the results were discussed and findings regarding the evaluation of the orthosis were summarized.

Chapter 2

Materials and methods

In this chapter, the pneumatically actuated knee orthosis, its force control mechanism and its assistive strategy are described. Thereafter, the other equipment and the way the data is recorded is described, followed by the experimental protocol. Finally, the steps taken in processing the data for analysis and the outcome variables are described.

2.1 Pneumatically actuated knee orthosis

In the research regarding the iMS approach, the pneumatically actuated knee orthosis shown in Figure 2.1 was developed [11]. Two equal pneumatic cylinders positioned in parallel are the source of force in the orthosis. To transfer force onto the body, each end of both cylinders is mounted to a shell by means of a hinge joint. The upper and lower shell, each with cutouts to allow for placement of surface electrodes for muscle activity measurements on the body, fit around the posterior side of the upper and lower leg respectively.
To compensate for the weight of the orthosis and to align the orthosis vertically, two connections to the body are present. First, the upper shell of the orthosis is attached to a band worn around the waist by means of straps. As a result, the weight from this shell is carried by the waist. Second, the lower shell rests on two slightly bendable pins that are attached to a shoe by means of heim joints. Due to the flexibility of the pins and the heim joints, this connection does not constrain movement of the ankle joint. With these connections, the orthosis can be aligned vertically along the posterior side of the leg such that the end of the cylinder from which the piston rod extends, is horizontally aligned with the knee joint.
The orthosis is further attached to the body with several types of flexible attachments. A velcro strap attached to each shell that goes around the leg keeps the shells attached to the leg. To restrict movement of the shells towards each other or sideways along the leg, six Boa closure systems with strategically positioned cables are present. The closure systems are located right above and below the knee joint at the anterior side of the leg and on the lateral and medial side of both the upper and lower shell. The closure systems on the upper and lower leg are connected to the two closure systems on the shell on that body part as well as to the anchor points medial and lateral to the knee joint. The closure systems above and below the knee and the medial and lateral anchor points have a velcro strap that goes around the leg.
A compressor supplies air to the orthosis through a 3/2-way solenoid valve which allows for disconnecting the orthosis from the air supply and connecting it to the atmosphere. Each chamber of the cylinder can be connected to the air supply to be able to both extend and retract. However, only one chamber is connected to the air supply while the other chamber is connected to the atmosphere simultaneously. This is done by means of a 5/3-way proportional valve. The chambers of both cylinders are attached to the same supply of air, which causes the cylinders to extend and retract in sync. As a result, the cylinders are always extended an equal amount.

Figure 2.1: A drawing (left) and a picture (right) of the pneumatically actuated knee orthosis used in the experimental validation. The orthosis consists of two pneumatic cylinders (A) and an upper (B) and lower shell (C). To compensate for its weight, the orthosis is attached to a waist band (D) and rests on two pins attached to a shoe (E). Five velcro straps (F) and six Boa closure systems (G) attach the orthosis to the body. Two anchor points (H) are present to attach the cables from the closure systems. A load cell (I) is present for each cylinder to measure the force and a pressure sensor (J) is present in the air supply for each cylinder to measure the air pressure. One of the cylinders has a linear Hall sensor (K) to measure the piston position. The four marker frames (X) of the motion capture system, described in Section 2.5.4 are attached to both of the shells and the anterior side of the upper and lower leg.

To be able to control the force delivered by the cylinders, the orthosis is equipped with several sensors. Each cylinder has an inline positioned load cell, that measures the force delivered by this cylinder. As a result, the total amount of force delivered by the orthosis is the sum of the force measured by both load cells. The pressure in the tubes right before entering each cylinder chamber is measured with a pressure sensor, as is the supply pressure right before the 5/3-way valve. The piston position of one of the cylinders is measured using a linear Hall sensor. Due to the design of the orthosis and both cylinders being attached to the same air supply, there is no need for measuring the extension of the other cylinder, since both cylinders will be equally extended at all times.

2.2 Force control mechanism

The force control mechanism of this orthosis is a combination of a sliding mode controller and a term proportional to the force tracking error. First, the mathematical model and the sliding mode controller, which are based on the approach in [27] and [28], are described. Thereafter, the term proportional to the force tracking error is described. Finally, the combination of this term and the sliding mode controller, that together make up the force control mechanism of the orthosis, is described.

2.2.1 Mathematical model

A mathematical model is created for the orthosis, of which a schematic representation is shown in Figure 2.2. In [27], an elaborate mathematical model of a pneumatic cylinder controlled by a proportional valve is presented. This mathematical model is used as the base for the mathematical model of this orthosis. The mathematical model consists of three separate parts describing the piston-load dynamics, the pressure dynamics throughout the tubes and cylinder chambers, and the valve dynamics.

2.2.1.1 Piston-load dynamics

The equation of motion for the piston-load dynamics of the orthosis is given by

$$(M_P + M_L)\,\ddot{x} + F_L = 2\,(P_1 A_1 - P_2 A_2 - P_a A_r)\,, \tag{2.1}$$

where M_P is the mass of the piston and rod assembly, M_L is the mass of the external load, i.e. the shell attached to the rod, x is the piston position, F_L is the external force acting on the system, i.e. the force exerted by the leg on the shell, P_1 and P_2 are the absolute pressures in the cylinder chambers, P_a is the atmospheric pressure, A_1 and A_2 are the effective areas of the cylinder chambers, and A_r is the cross-sectional area of the rod. In this equation, the pressures P_1 and P_2 cannot be smaller than the atmospheric pressure P_a and cannot be larger than the supply pressure P_s.
It differs from the equation of motion stated in [27] in three ways. First, the Coulomb friction force and viscous friction coefficient are not incorporated. In [27], the Coulomb friction force and viscous friction coefficient are determined experimentally. Since it was assumed that these terms had little influence on the model, the values were neglected instead of determined experimentally. Second, it is not possible to distinguish between the force exerted by the leg on the orthosis, F_L, and the force exerted by the orthosis on the leg, $(M_P + M_L)\,\ddot{x}$. The force sensor located between the end of the piston rod and the shell measures the resulting force, i.e. a combination of both forces. The complete left-hand side of Equation 2.1 therefore represents the force delivered by the cylinders. Third, the right-hand side of the equation representing the force delivered by the pneumatic actuator is multiplied by two, since the orthosis consists of two identical cylinders.

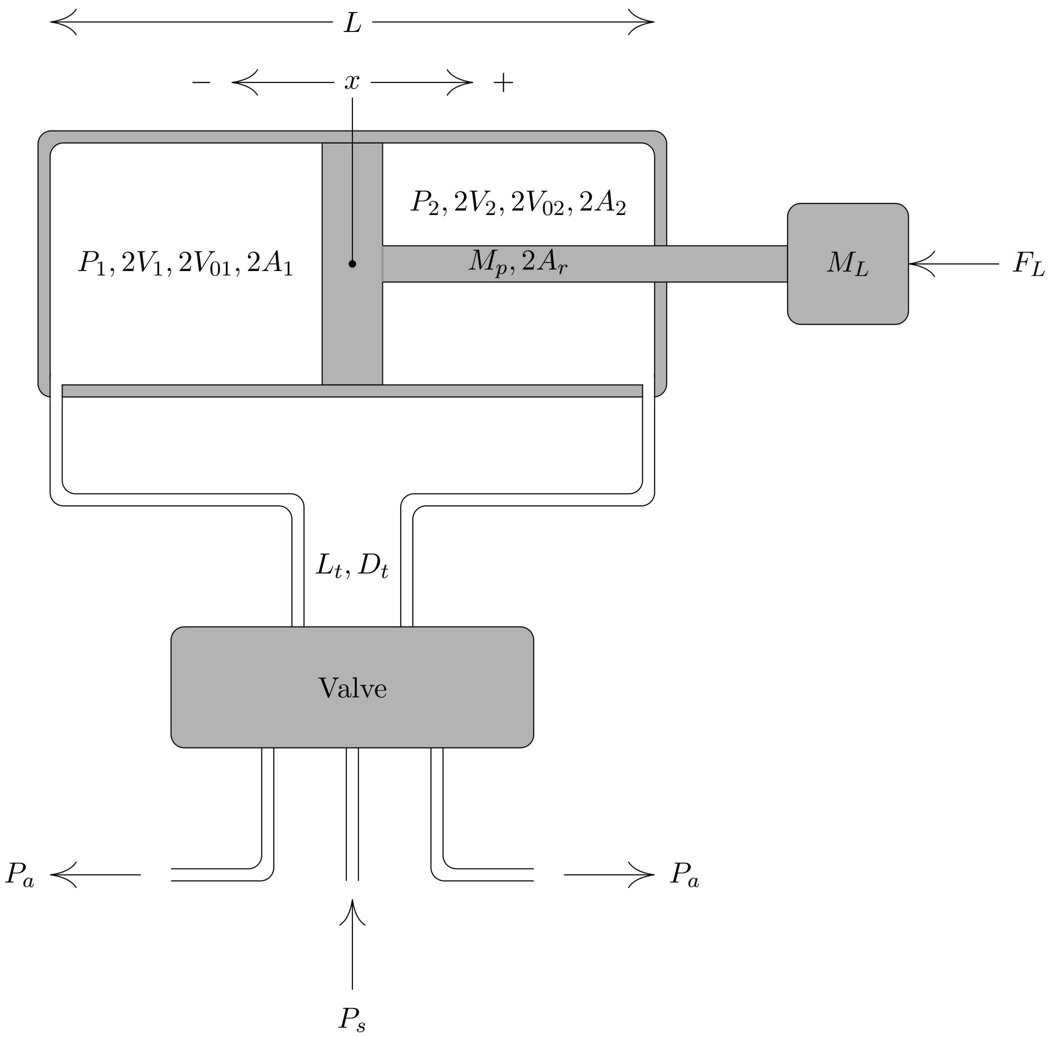

Figure 2.2: A schematic representation of the orthosis consisting of two pneumatic cylinders, represented as one with doubled effective areas for simplicity, connecting tubes, and a 5/3-way proportional valve.

2.2.1.2 Pressure dynamics

The time derivative of the pressure in a chamber of the pneumatic cylinder is given by

$$\dot{P}_i = \frac{RT}{2\left(V_{0i} + V_t + A_i\left(\frac{1}{2}L \pm x\right)\right)}\left(\alpha_{in}\dot{m}_{in} - \alpha_{ex}\dot{m}_{ex}\right) \pm \alpha\frac{P_i A_i}{V_{0i} + V_t + 2A_i\left(\frac{1}{2}L \pm x\right)}\dot{x}, \tag{2.2}$$

where P_i is the pressure in the chamber specified by i, either 1 or 2, R is the ideal gas constant, T is the temperature, V_{0i} is the inactive volume of the specified chamber, V_t is the volume of the tube connecting the valve to the chamber, A_i is the effective area of the specified chamber, L is the stroke of the piston, x is the piston position, α_{in}, α_{ex} and α are the heat transfer coefficients for charging and discharging the specified chamber and for compression and expansion due to piston movement respectively, and $\dot{m}_{in}$ and $\dot{m}_{ex}$ are the mass flows entering and leaving the specified chamber respectively. The volume of the tube V_t is given by

$$V_t = \frac{\pi}{4}D_t L_t, \tag{2.3}$$

where D_t is the diameter of the tube and L_t is the length of the tube.
This pressure dynamics equations differs from the equation stated in [27] in two ways. First, since the orthosis consists of two identical cylinders, the volume of each chamber is multiplied by two. This multiplication by two cancels out in the last fraction, since the effective area of the cylinder chamber is in both the numerator and the denominator. Second, the leakage between the cylinder chambers is neglected since the cylinders of the orthosis are not low friction cylinders [27].
The equations for the mass flow $\dot{m}_{in}$ and $\dot{m}_{ex}$ entering and leaving a cylinder chamber respectively are given by

$$\dot{m}_{in} = \phi_{in}\dot{m}_{v_{in}}\left(t - \tau\right) \tag{2.4}$$

and

$$\dot{m}_{ex} = \phi_{ex}\dot{m}_{v_{ex}}\left(t - \tau\right), \tag{2.5}$$

where ϕ_{in} and ϕ_{ex} are the attentuations of the air flow in the tube towards the orthosis and from the orthosis respectively, $\dot{m}_{v_{in}}$ and $\dot{m}_{v_{ex}}$ are the mass flows through the input and exhaust path of the valve respectively, and $\tau = L_t/c$ is the time it takes for the air to travel through the tube.
The attentuation of the air flow through a tube ϕ is given by

$$\phi = e^{-R_t RT/2P \;\; L_t/c}, \tag{2.6}$$

where R_t is the tube resistance, R is the ideal gas constant, T is the temperature, P is the pressure at the end of the tube, L_t is the length of the tube, and c is the speed of sound in air. For fully developed laminar flow, which is assumed to be the case, similar to [27], $R_t = 32\mu/D_t^2$ with μ the dynamic viscosity of air and D_t the inner diameter of the tube.
The mass flows through the input and exhaust path of the valve, $\dot{m}_{v_{in}}$ and $\dot{m}_{v_{ex}}$ respectively, are given by

$$\dot{m}_{v_{in}} = C_f A_{v_{in}}\frac{P_s}{\sqrt{T}}\dot{m}_r\left(P_s, P_i\right) \tag{2.7}$$

and

$$\dot{m}_{v_{ex}} = C_f A_{v_{ex}}\frac{P_i}{\sqrt{T}}\dot{m}_r\left(P_i, P_a\right), \tag{2.8}$$

where C_f is a non-dimensional discharge coefficient, $A_{v_{in}}$ and $A_{v_{ex}}$ are the valve opening areas of the input and exhaust path respectively, P_s is the supply pressure, P_i is the pressure in the chamber specified by i, either 1 or 2, P_a is the atmospheric pressure, T is the temperature, and $\dot{m}_r$ a function of two pressures. This function $\dot{m}_r$ is given by

$$\dot{m}_r = \begin{cases} C_f \sqrt{\frac{k}{R}\left(\frac{2}{k+1}\right)^{k+1/k-1}} \frac{P_u}{\sqrt{T}} & \text{if } \frac{P_d}{P_u} \leq \frac{2}{k+1}^{k/k-1} \\ C_f \sqrt{\frac{2k}{R(k-1)}} \frac{P_u}{\sqrt{T}}^{1/k} \sqrt{1 - \frac{P_d}{P_u}^{(k-1)/k}} & \text{if } \frac{P_d}{P_u} > \frac{2}{k+1}^{k/k-1}, \end{cases} \tag{2.9}$$

where k is the specific heat ratio, R is the ideal gas constant, P_u and P_d are the upstream and downstream pressures of the tube respectively, and T is the temperature.
Combining Equations 2.2, 2.4 and 2.5 results in the equations for the pressure in each cylinder chamber given by

$$\begin{aligned} \dot{P}_1 =& \frac{C_f R\sqrt{T}}{2\left(V_{01} + V_t + A_1\left(\frac{1}{2}L + x\right)\right)} \left(\alpha_{in}\phi_{in}\overline{A_{v1_{in}}} P_s \dot{m}_r\left(P_s, \overline{P_1}\right) - \alpha_{ex}\phi_{ex}\overline{A_{v1_{ex}} P_1}\dot{m}_r\left(\overline{P_1}, P_a\right)\right) \\ &- \alpha\frac{P_1 A_1}{V_{01} + V_t + A_1\left(\frac{1}{2}L + x\right)}\dot{x} \end{aligned} \tag{2.10}$$

and

$$\begin{aligned} \dot{P}_2 =& \frac{C_f R\sqrt{T}}{2\left(V_{02} + V_t + A_2\left(\frac{1}{2}L - x\right)\right)} \left(\alpha_{in}\phi_{in}\overline{A_{v2_{in}}} P_s \dot{m}_r\left(P_s, \overline{P_2}\right) - \alpha_{ex}\phi_{ex}\overline{A_{v2_{ex}} P_2}\dot{m}_r\left(\overline{P_2}, P_a\right)\right) \\ &+ \alpha\frac{P_2 A_2}{V_{02} + V_t + A_2\left(\frac{1}{2}L - x\right)}\dot{x}, \end{aligned} \tag{2.11}$$

where the variables with overbars are delayed by time τ.

2.2.1.3 Valve dynamics

In [27], equations for the effective areas for the input and exhaust paths of the valve were derived. In their setup, a four-way proportional spool valve, actuated by voice coils was used. Since the orthosis is equipped with a different type of valve, the equation for the valve effective areas stated in [27] could not be used to derive that equation for the 5/3-way proportional valve.
A schematic representation of the 5/3-way proportional valve used in the orthosis is shown in Figure 2.3. In the orthosis, port 1 is connected to the air supply and ports 3 and 5 are connected to the atmosphere without any tubes. Port 2 and 4 are connected to chamber 2 and 1 of the cylinders respectively. When chamber 1 is connected to the air supply and chamber 2 is connected to the atmosphere, the cylinder extends. When chamber 1 is connected to the atmosphere and chamber 2 is connected to the air supply, the cylinder retracts. When both cylinder chambers are connected to the atmosphere, the cylinder does not extend or retract.
The 5/3-way proportional valve has a position controlled spool that connects the air supply to one of the ports connected to a cylinder chamber [29]. The input of the controller of the spool position is a voltage signal and the output is the cross-sectional area of the port that it connects to. The larger the cross-sectional area of the port, the higher the flow rate of air into the cylinder chamber connected to the air supply and out of the cylinder chamber connected to the atmosphere. This relation between setpoint voltage and flow rate is shown in Figure 2.4. The position of the spool does not only determine whether or not the cylinder extends or retracts, but also the speed of this movement, since a higher flow rate results in a faster movement of the piston.
The equation of the valve dynamics in [27] describes the relation between the setpoint voltage and the resulting cross-sectional area of the opening of the valve. Therefore, the flow rate shown

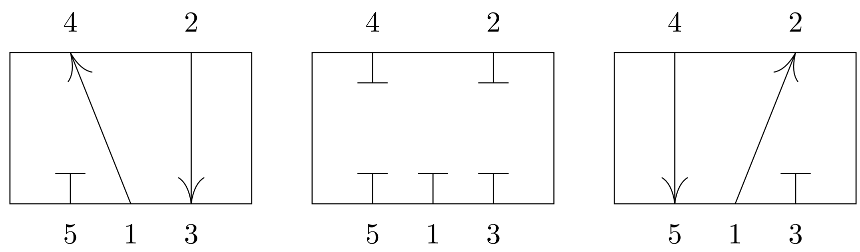

Figure 2.3: A schematic representation of the three ways in which the five ports of the 5/3-way proportional valve, used in the orthosis, can be connected. Port 1 is connected to the air supply, port 3 and 5 are connected to the atmosphere and port 2 and 4 are connected to separate parts of the device. In the situation on the left, port 4 is connected to the supply pressure and port 2 is connected to the atmosphere, causing the pressure in the part of the device connected to port 4 to rise and in the part connected to port 2 to drop. In the situation on the right, port 4 is connected to the atmosphere and port 2 is connected to the supply pressure, causing the pressure in the part of the device connected to port 4 to drop and in the part connected to port 2 to rise. In the situation in the middle, none of the ports are connected, causing the pressure in both parts of the device to remain equal.

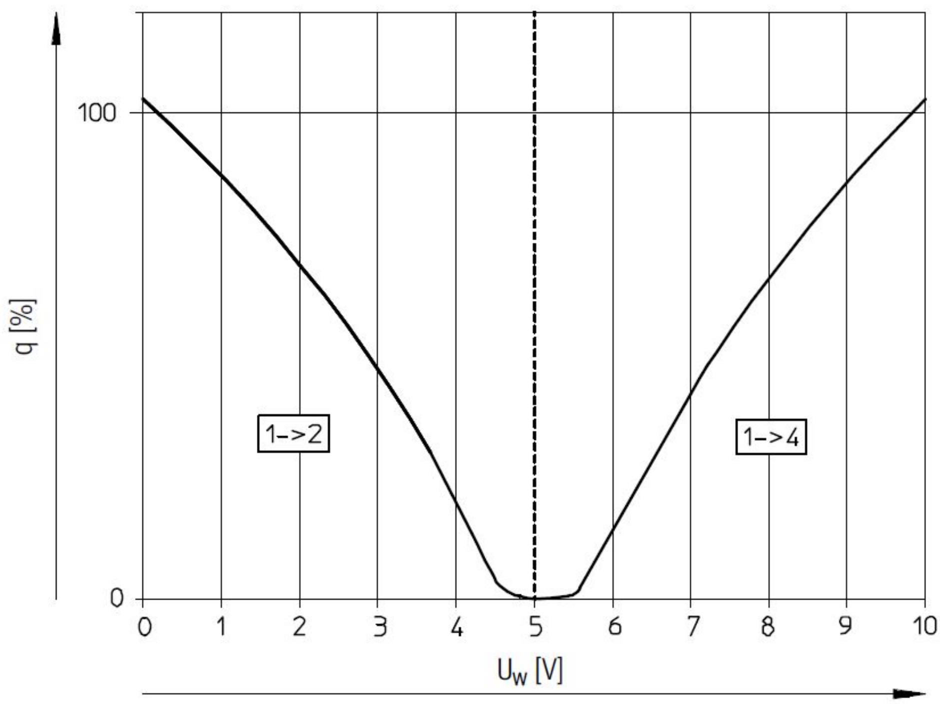

Figure 2.4: The relation between setpoint voltage and flow rate percentage for a flow from 6 to 5 bar for the 5/3-way proportional valve in the orthosis. Reprinted from [29].

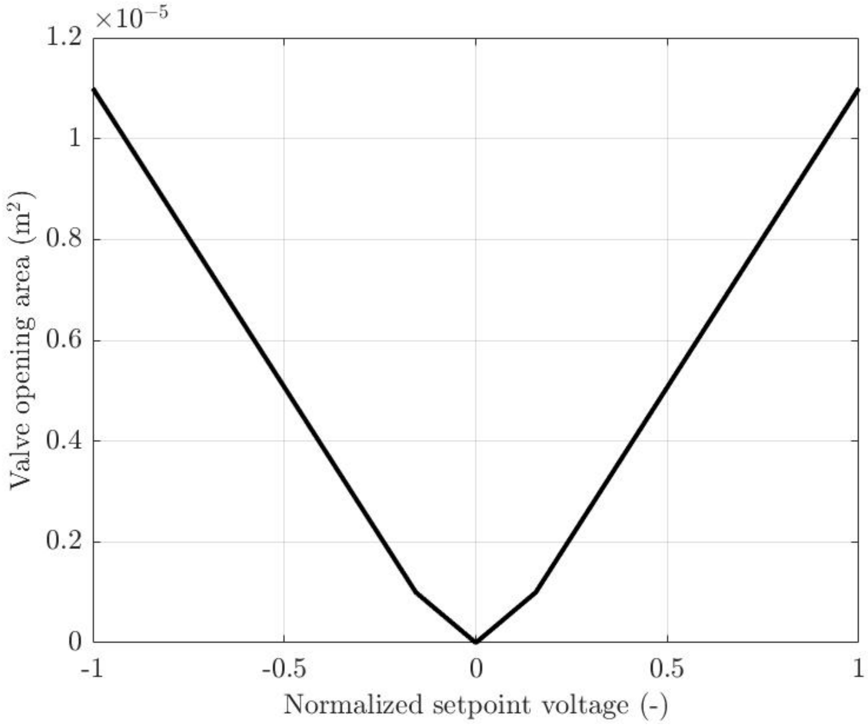

Figure 2.5: The modeled relation between setpoint voltage and the cross-sectional area of the opening of the valve for the 5/3-way proportional valve in the orthosis.

in Figure 2.4 needs to be converted to a cross-sectional area to use this equation in the creation of a mathematical model of the orthosis. It is assumed that the percentage of the flow rate corresponds linearly with the percentage of the maximum cross-sectional area of the opening of the valve. As a result, the relation shown in Figure 2.4 can be mapped to the maximum cross-sectional area of the opening of the valve. For simplicity, the relation between the normalized setpoint voltage and the valve opening area is divided into two linear parts and is shown in Figure 2.5 where the setpoint voltage range from 0 to 10 V is normalized to a range from -1 to 1. When the normalized setpoint voltage is smaller than 0, air flows into chamber 2 and out of chamber 1, decreasing the force exerted by the orthosis. When the normalized setpoint voltage is larger than 0, air flows into chamber 1 and out of chamber 2, increasing the force exerted by the orthosis. For a normalized setpoint voltage of 0, no air will flow in or out each chamber, maintaining the force exerted by the orthosis.

2.2.2 Sliding mode controller

A sliding mode controller is created for the orthosis, which is known to be robust for model uncertainies and to have a high performance in nonlinear systems, such as a pneumatic cylinder [27, 28, 30, 31]. This sliding mode controller is based on the reduced order sliding mode controller described in [28]. The reduced order controller is used, since the valve dynamics are not described using a differential equation as in [27], but rather as a relation between setpoint voltage and valve opening area. Using the reduced order controller only slightly alters the performance up to frequencies of 20 Hz, a threshold that should not be exceeded during treadmill walking [28]. The steps taken to derive the equations for the controller are performed as described in [28], but with the mathematical model of the orthosis described in Section 2.2.1.
The force delivered by the orthosis is derived from Equation 2.1. The resulting equation for the actuator force F_a is given by

$$F_a = 2\left(P_1 A_1 - P_2 A_2 - P_a A_r\right), \tag{2.12}$$

where P_1 and P_2 are the absolute pressures in the cylinder chambers, P_a is the atmospheric pressure, A_1 and A_2 are the effective areas of the cylinder chambers, and A_r is the cross-sectional area of the rod.
The tracking error $\tilde{F}$ of the sliding mode controller, which is equal to the sliding function s, is given by

$$\tilde{F} = F_a - F_d = s, \tag{2.13}$$

where F_d is the desired force that should be delivered by the orthosis. The controller must set the sliding function s equal to zero in order to control the orthosis. The resulting sliding mode equation, the time derivative of s, is given by

$$\dot{s} = 2\left(\dot{P}_1 A_1 - \dot{P}_2 A_2\right) - \dot{F}_d. \tag{2.14}$$

By substituting Equations 2.10 and 2.11 into Equation 2.14 and setting $\dot{s}$ equal to zero, the equations for the valve opening areas for the inlet and exhaust path are given by

$$A_{v_{in}} = \begin{cases} \dfrac{2\alpha\left(A_1^2 V_2 P_1 + A_2^2 V_1 P_2\right)\dot{x} + \dot{F}_d V_1 V_2}{C_f R\sqrt{T}\left(A_1 V_2 \alpha_{in}\phi_{in} P_s \dot{m}_r\left(P_s, P_1\right) + A_2 V_1 \alpha_{ex}\phi_{ex} P_2 \dot{m}_r\left(P_2, P_a\right)\right)} & \text{if } \tilde{F} < 0 \\ 0 \quad \text{if } \tilde{F} \geq 0 \end{cases} \tag{2.15}$$

and

$$A_{v_{ex}} = \begin{cases} -\dfrac{2\alpha\left(A_1^2 V_2 P_1 + A_2^2 V_1 P_2\right)\dot{x} + \dot{F}_d V_1 V_2}{C_f R\sqrt{T}\left(A_1 V_2 \alpha_{ex}\phi_{ex} P_1 \dot{m}_r\left(P_1, P_a\right) + A_2 V_1 \alpha_{in}\phi_{in} P_s \dot{m}_r\left(P_s, P_2\right)\right)} & \text{if } \tilde{F} > 0 \\ 0 \quad \text{if } \tilde{F} \leq 0, \end{cases} \tag{2.16}$$

where $V_1 = 2\left(V_{01} + V_t + A_1\left(\frac{1}{2}L + x\right)\right)$ and $V_2 = 2\left(V_{02} + V_t + A_2\left(\frac{1}{2}L - x\right)\right)$, ϕ as shown in Equation 2.6 and $\dot{m}_r\left(P_u, P_d\right)$ as shown in Equation 2.9. It is assumed that the inlet and exhaust area of the valve are equal, $A_{v1_{in}} = A_{v2_{ex}} = A_{v_{in}}$ and $A_{v1_{ex}} = A_{v2_{in}} = A_{v_{ex}}$ and that air can only flow into one chamber at a time, $A_{v_{in}} A_{v_{ex}} = 0$.

2.2.3 Proportional term

Since the sliding mode controller is only concerned with the time derivative of the force tracking error, a term proportional to the force tracking error is present in the force control mechanism of the orthosis as well. The equation of this propertional term A_{v_p} is given by

$$A_{v_p} = -A_{v_{pmax}} \frac{\tilde{F}}{F_{ad}}, \tag{2.17}$$

where $A_{v_{pmax}}$ is the maximal valve area for the proportional part of the valve area, $\tilde{F}$ is the force tracking error, and F_{ad} is the admissible force error. The value of the proportional term is bound between 0 and $A_{v_{pmax}}$.

2.2.4 Combined force control mechanism

Combining Equations 2.15 and 2.16 regarding the sliding mode control and Equation 2.17 regarding the proportional control results in the equation for the force control mechanism of the orthosis given by

$$A_v = \begin{cases} A_{v_{in}} + A_{v_p} & \text{if } \tilde{F} < 0 \\ A_{v_{ex}} + A_{v_p} & \text{if } \tilde{F} > 0 \\ 0 \quad \text{if } \tilde{F} = 0, \end{cases} \tag{2.18}$$

Table 2.1: Variables in the equations of the force control mechanism of the pneumatically actuated knee orthosis.

Variable	Description	Unit
$A_{v_{in}}$	Valve cross-sectional area for air flow into chamber 1 and out of chamber 2, increasing the force delivered by the orthosis	m^2
$A_{v_{ex}}$	Valve cross-sectional area for air flow into chamber 2 and out of chamber 1, decreasing the force delivered by the orthosis	m^2
$\tilde{F}$	Force tracking error	N
F_d	Desired force	N
P_1	Absolute pressure in chamber 1	Pa
P_2	Absolute pressure in chamber 2	Pa
x	Piston position	m

where A_v is the desired valve area that is bound between 0 and $A_{v_{max}}$. The modeled relation between the setpoint voltage and cross-sectional area of the opening of the valve, shown in Figure 2.5, is used to convert the desired area to a setpoint voltage for the 5/3-way proportional valve. This valve allows air to flow into the desired chamber to minimize the force tracking error and therefore control the force delivered by the orthosis.
The variables used in Equation 2.18 and its subequations are shown in Table 2.1. The constants and their values used in these equations are shown in Table 2.2.

2.3 Assistive strategy

The orthosis has an assistive strategy to assist the wearer during walking. It depends on the knee joint angle, the lever arm, the gait phase and the estimated duration of the stance phase of the right leg. The assistive strategy is therefore robust for changes in gait dynamics and it does not force the gait dynamics to follow a predefined pattern. First, the calculation of these four variables from the data recorded during the experimental validation is described. Thereafter, it is described how the assistive force was calculated from these values.

2.3.1 Knee joint angle

The knee joint angle θ, in degrees, which depends on the piston position, is given by

$$\theta = 2\,(90 - \alpha - \beta) = 2\left(90 - \arctan\left(\frac{d}{h}\right) - \arcsin\left(\frac{l_{min} + x}{2\sqrt{h^2 + d^2}}\right)\right), \tag{2.19}$$

where d is the perpendicular distance from the leg segment axis to the posterior side of the segment, h is the distance from the knee joint axis to the attachment of the cylinder, parallel to the segment axis, l_{min} is the minimal length of the cylinder when the piston position x is zero, and α and β are two angles defined to clarify the calculation. The distances d and h are assumed to be equal for both the upper and lower leg and are assumed to hold for all subjects participating in the experiments. The lengths and distances used in this equation and the knee joint angle itself are illustrated in Figure 2.6a.

2.3.2 Lever arm

The lever arm for the force of the orthosis acting on the knee joint, which depends on the piston position, is given by

$$a = \sqrt{\sqrt{h^2 + d^2} - \left(\frac{l_{min} + x}{2}\right)^2}, \tag{2.20}$$

Table 2.2: Constants in the equations of the force control mechanism of the pneumatically actuated knee orthosis.

Constant	**Description**	**Value**	**Unit**
A_r	Effective area of the piston rod	$5.03 \cdot 10^{-5}$	m^2
$A_{v_{max}}$	Maximum valve cross-sectional area	$1.1 \cdot 10^{-5}$	m^2
$A_{v_{p_{max}}}$	Part of the maximum valve cross-sectional area used in the proportional part of the force control mechanism	$0.9 \cdot 10^{-5}$	m^2
A_1	Effective area of chamber 1	$3.14 \cdot 10^{-4}$	m^2
A_2	Effective area of chamber 2	$2.64 \cdot 10^{-4}$	m^2
α	Heat transfer coefficient for compression and expansion due to piston movement	0.75	-
α_{ex}	Heat transfer coefficient for discharging the chamber	1	-
α_{in}	Heat transfer coefficient for charging the chamber	1.4	-
c	Speed of sound in air	343	m/s
C_f	Non-dimensional discharge coefficient	0.25	-
D_t	Inner tube diameter	$5.5 \cdot 10^{-3}$	m
F_{ad}	Admissible force tracking error	30	N
k	Specific heat ratio	1.401	-
L	Piston stroke	0.15	m
L_t	Tube length	0.35	m
μ	Dynamic viscosity of air	$1.85 \cdot 10^{-5}$	$N \cdot s/^2$
P_a	Atmospheric pressure	101325	Pa
P_s	Supply pressure	900000	Pa
R	Ideal gas constant	287.058	J/kg·K
T	Temperature	293.15	K
V_{01}	Inactive volume of chamber 1	$1.57 \cdot 10^{-6}$	m^3
V_{02}	Inactive volume of chamber 2	$1.32 \cdot 10^{-6}$	m^3

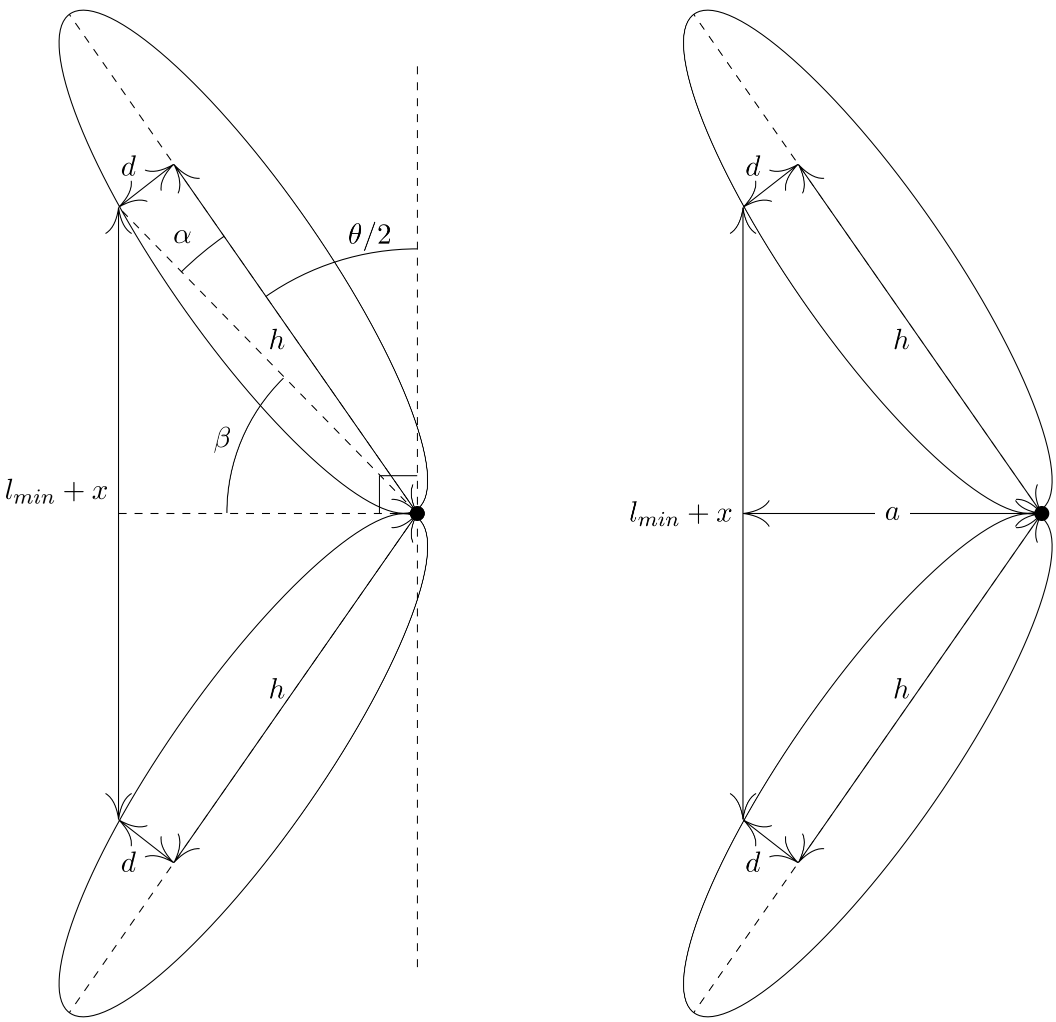

(a) Calculation of the knee joint angle θ

(b) Calculation of the lever arm a

Figure 2.6: Schematic representations of the lengths and distances used in calculation of the knee joint angle in Equation 2.19 and the lever arm in Equation 2.20.

which uses the same lengths and distances used in the knee joint angle calculation. The lengths and distances used in this equation and the lever arm itself are illustrated in Figure 2.6b.

2.3.3 Gait phase

A gait cycle is defined to consist of four successive gait phases: double stance with the right foot in front, single stance of the right leg, i.e. swing of the left leg, double stance with the left foot in front, and single stance of the left leg, i.e. swing of the right leg. The start of a gait cycle is defined as the heel strike of the right foot.
The gait phase is determined using the force plates under each of the two belts of the split belt treadmill. As the subject walks with the left and right foot on the left and right belt of the treadmill respectively, the gait phase is determined by the measured ground reaction force of the force plate under each belt. During the single stance phases, the measured ground reaction force is non-zero for one plate and zero for the other plate. The leg that is in single stance phase is in contact with a belt, causing a non-zero ground reaction force on the corresponding plate. During the double stance phases, the measured ground reaction forces are non-zero for both plates, as both feet are in contact with a belt. To distinguish between the double stance phases, the previous single stance phase is taken into account, since the order of the gait phases is always

equal during normal walking. After single stance of the right leg, the following double stance phase is with the right foot in front whereas after single stance of the left leg, the following double stance phase is with the left leg in front.

2.3.4 Stance phase duration

The stance phase of the right leg consists of three gait phases: double stance with the right foot in front, single stance of the right leg, and double stance with the left foot in front. It starts at heel strike of the right foot and lasts until toe-off of the right foot. The duration of the stance phase of the right leg is estimated by taking the median of the five previous durations of this phase.

2.3.5 Desired force

The orthosis can operate in minimal impedance mode and assistive mode. During the minimal impedance mode, the desired force and time derivative of the desired force are both always zero. During the assistive mode, which adheres to the iMS approach, the desired force is positive or zero, while the time derivative of the desired force is zero. Since the force delivered by the orthosis does not act in line with the knee joint, it is actually a desired torque acting on the knee joint.
The desired torque in the assistive mode is different during the swing phase of the right leg compared to the stance phase of the right leg. Throughout the stance phase of the right leg, the orthosis should act as a spring with a certain spring constant k. This corresponds to a desired torque linear to the knee joint angle. This torque is zero if the knee joint angle is zero and non-zero otherwise. Therefore, when the knee joint angle is non-zero, the orthosis will deliver a positive torque on the knee joint in an attempt to achieve a knee joint angle of zero degrees. During the swing phase of the right leg, the desired torque is zero as it is while in minimal impedance mode.
The knee joint angle will not be exactly zero degrees at the start and end of the stance phase, i.e. heel strike and toe-off of the right foot respectively [32, 33]. As a result, the desired torque would instantly go from zero to a non-zero positive torque at heel strike of the right foot and from a non-zero positive torque to zero at toe-off of the right foot. This abrupt change in desired torque leads to a similar abrupt change in the desired force that would be difficult for the force control mechanism to track.
To prevent this abrupt change in desired torque, it is multiplied by a weighting function that first gradually increases from zero to one, then stays constant at one, and finally gradually decreases from one to zero again. This weighting function is shown in Figure 2.7. For the increase and decrease, whose durations are equal, a Guassian function is used to make these transitions seamless.
The duration of the stance phase of the right leg is estimated to predict the start of the decrease of the weighting function. If the stance phase would last shorter than estimated, the desired torque could still be larger than zero after toe-off. To decrease the chance of having a non-zero torque at the start of the swing phase, the last part of the weighting function is started a fixed period of time before it would need to start to have a desired torque of zero at the estimated end of the stance phase. This shortening of the duration the weighting function is non-zero, makes the assistive strategy more robust for changes in step length.
The desired torque T_d is given by

$$T_d = \begin{cases} \theta k \frac{0.1}{\sigma\sqrt{2\pi}} e^{-\frac{1}{2}\left(\frac{t-\mu}{\sigma}\right)^2} \quad \text{if } t < t_a \\ \theta k \quad \text{if } t_a < t < t_s - t_a - t_b \\ \theta k \frac{0.1}{\sigma\sqrt{2\pi}} e^{-\frac{1}{2}\left(\frac{t-(\mu+t_s-2t_a-t_b)}{\sigma}\right)^2} \quad \text{it } t > t_s - t_a - t_b, \end{cases} \tag{2.21}$$

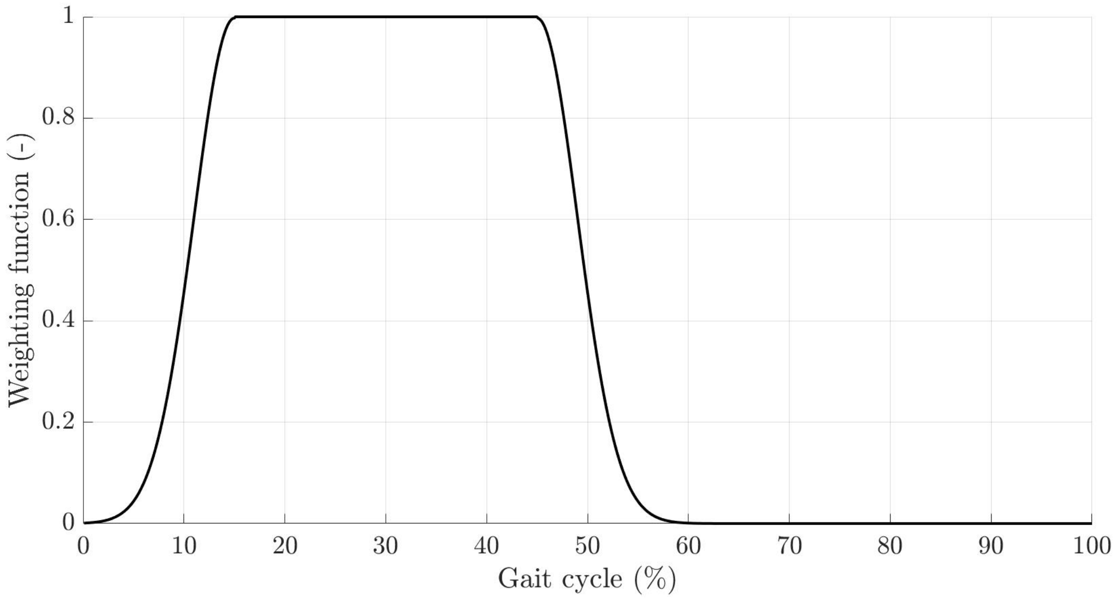

Figure 2.7: A visualization of the weighting function in the assistive strategy. For this particular weighting function, the stance phase starts at 0% of the gait cycle and lasts until 65% of the gait cycle.

Table 2.3: Variables in the equations of the assistive strategy of the pneumatically actuated knee orthosis.

Variable	Description	Unit
a	Moment arm	m
t	Time since the start of the stance phase	s
t_s	Estimated duration of the stance phase	s
θ	Knee joint angle	degrees
x	Piston position	m

where θ is the knee joint angle, k is the spring constant, μ and σ are constants in the weighting function, t is the time since the start of the stance phase, t_a is the time in which the weighting function increases from zero to one or decreases from one to zero, t_s is the estimated duration of the stance phase, and t_b is the period of time the decrease of the weighting function is advanced with to be more robust to changes in the duration of the gait cycle.
The desired force F_d that is an input for the force control mechanism, described in Section 2.2, is given by

$$F_d = \frac{T_d}{a}, \tag{2.22}$$

where T_d is the desired torque and a is the lever arm.
The variables used in Equation 2.22 and its subequations are shown in Table 2.3. The constants and their values used in these equations are shown in Table 2.4.

2.4 Subjects

Five healthy subjects, two male, three female, participated in the experimental validation after giving informed consent. For a subject to participate, the orthosis had to fit correctly around the leg and the range of motion of the knee joint should not be limited by the orthosis. Indeed this was the case for all subjects that were asked to participate.

Table 2.4: Constants in the equations of the assistive strategy of the pneumatically actuated knee orthosis.

Constant	Description	Value	Unit
d	Perpendicular distance from the segment axis to the posterior side of the segment	0.089	m
h	Distance from the knee joint axis to the attachment of the cylinder	0.215	m
k	Spring constant	0.2	N/m
l_{min}	Minimal cylinder length	0.28	m
μ	Mean in Gaussian weighting function	0.15	-
σ	Standard deviation in Gaussian weighting function	0.04	-
t_a	Duration the weighting function increases from zero to one or decreases from one to zero	0.15	s
t_b	Duration as a buffer to be robust against changes in gait cycle duration	0.05	s

2.5 Equipment and recordings

Besides the orthosis, described in Section 2.1, several pieces of equipment were used during the experimental validation. These pieces of equipment are described, together with the frequency at which data was collected. If applicable, the way the equipment was used during the experimental validation is described as well.

2.5.1 Orthosis

The mathematical model of the orthosis, its force control mechanism and its assistive strategy were modeled in Simulink (The Mathworks, Natick, US). Using a target PC with Simulink RealTime, equipped with data acquisition cards, an interface with the orthosis was created. The data measured by the sensors attached to the orthosis was recorded at 1000 Hz.

2.5.2 Treadmill

During the experiment, the subjects walked on a custom Y-mill (Motekforce Link, Culemborg, The Netherlands) with two separate belts, one for each foot. Each belt was equipped with a force place that measured the ground reaction forces and torques at 1000 Hz.

2.5.3 Muscle activity measurement

Using the Delsys Trigno wireless EMG system (Delsys, Natick, US), the muscle activity of several muscles in the right leg was measured at 1000 Hz. The surface electrodes were placed on the quadriceps femoris rectus femoris and quadriceps femoris vastus lateralis, responsible for extension of the knee, and on the gastrocnemius medialis and biceps femoris, responsible for flexion of the knee [34].
Before placing the electrodes, the area was marked and the orthosis was put on to check if the electrode would not lie beneath a shell or strap. If so, another position was found for the electrode such that it would not be touched by the shell. After the orthosis was put on, the placement of the electrodes was tested by activating each muscle and manually investigating the measured activity [34].

2.5.4 Motion capture

Motion of the orthosis, and the leg it is attached to, was measured at 100 Hz using the Qualisys motion capture system (Qualisys AB, Göteborg, Sweden). Four marker frames, consisting of

five randomly distributed passive markers, were used. Two marker frames were attached to the posterior side of the upper and lower shell, above and below the connection with the cylinders respectively. After putting on the orthosis, the other two marker frames were attached to the anterior side of the upper and lower leg, in between the straps from the shell and the Boa closure systems on that body part. The location of the marker frames is shown in Figure 2.1.
The Qualisys Track Manager was configured to identify the markers of each marker frame during the trials. However, when markers were out of reach of the cameras, they were not identified and when the markers were in reach again, they were potentially misidentified. Therefore, all Qualisys data was manually checked for unidentified and misidentified markers after the experimental validation and complemented or corrected if needed.

2.5.5 Synchronization

The data from the sensors of the orthosis, the force plates in the treadmill and the surface electrodes of the EMG system were collected in the Simulink model. The data from the motion capture system was recorded separately and at a different frequency.
To analyze the data, the data from these two sources had to be synchronized by means of a random synchronization signal. The Simulink model generated a synchronization signal that was forwarded to the motion capture system as an analog input. As a result, both data structures contained the same synchronization signal which allowed for synchronization. Before combining the two data structures, the data collected in the Simulink model had to be resampled to 100 Hz to correspond with the sampling frequency of the motion capture system.

2.6 Experimental protocol

Each experiment started with a static trial in which the subject was standing straight in the center of the treadmill. The orthosis was not active during this trial, meaning that no air was supplied to the orthosis and therefore no force could be delivered by the orthosis. 20 seconds of data was recorded in this static trial.
Thereafter, six trials were performed in which the subject walked on the treadmill. In three of these trials the orthosis was in minimal impedance mode, while in the other three trials the orthosis was in assistive mode. The order of these six trials was randomized.
Each walking trial was performed in a silimar way by executing the following steps. The trial started with the orthosis in minimal impedance mode and the treadmill off. First, the speed of the treadmill was gradually increased to 2 km/h. Second, the correct mode of the orthosis was selected for the trial. In case it was a trial with the orthosis in minimal impedance mode, the mode was already correct. In case it was a trial with the orthosis in assistive mode, the assistive mode had to be enabled. Third, the subject walked on the treadmill at a speed of 2 km/h with the orthosis in the correct mode for one minute. Fourth, data was recorded for 20 seconds. Fifth, the mode of the orthosis was set to minimal impedance. In case it was a trial with the orthosis in minimal impedance mode, the mode was already correct. In case it was a trial with the orthosis in assistive mode, the assistive mode was disabled. Finally, the speed of the treadmill was gradually decreased until it stopped.

2.7 Data analysis

Processing of the data recorded during this experimental validation was done using Matlab 2016b (The Mathworks, Natick, US). First, the processing of the recorded data is described, followed by the outcome variables of this experimental validation.

2.7.1 Data processing

Before synchronizing the two data structures for each trial, the muscle activity data was processed using standard filtering and rectifying methods [35]. First, a 20 Hz second order zero-phase high-pass filter was applied to the data. Thereafter, the data was rectified. Finally, a second order zero-phase low-pass filter with a cut-off frequency of 6 Hz was applied.
After synchronization, the motion capture data was interpolated using the spline method to account for missing data points due to markers that were not captured by any of the cameras at some point during the trial. This was the final processing step performed on the data from the static trial. The rest of the processing steps were only performed for the walking trials.
The combined data structure with a sampling frequency of 100 Hz, was split into gait cycles based on the gait phase. The gait cycle is defined to start with heel strike of the right foot, as described in Section 2.3.3. The uncompleted gait cycles at the start and end of a trial were removed from the data structure. The gait cycles from the three walking trials with the orthosis in the same mode were grouped. The data was time-interpolated to 200 data points per gait cycle.
Finally, additional processing was done on parts of the data structure. First, the gait phase signal was rounded to whole numbers. Second, the muscle activity data of each muscle during a gait cycle was normalized with the maximum activity of that muscle in the minimal impedance trials averaged over the gait cycles.
For all data, except the force-related data, the subject average was calculated by averaging the data over the gait cycles. Thereafter, those subject averages were averaged as well, thereby compensating for the possibility of a deviating number of gait cycles between subjects.

2.7.2 Outcome variables

The performance of the force control mechanism of the orthosis is evaluated by means of the force tracking error. The force tracking error was calculated by subtracting the desired force from the delivered force. The force tracking error during the gait cycle is an outcome variable, as is the root mean square of the force tracking error during the gait cycle, the stance phase, and the swing phase. The root mean square of the force tracking error is used to compare the force tracking error between the minimal impedance mode and assistive mode trials.
The performance of the assistive strategy is evaluated by means of its interference with gait, specifically the knee joint angle and the gait phase duration. The knee joint angle was calculated from the piston position. The gait phase duration was calculated from the detected gait phases during the gait cycle, as a percentage of the duration of the gait cycle. The knee joint angle during the gait cycle is an outcome variable, as are the durations of the four gait phases.
The performance of the assistive strategy is evaluated by means of its interference with the muscle activity of several muscles in the right leg. The muscle activity of the gastrocnemius medialis, biceps femoris, quadriceps femoris rectus femoris, and quadriceps femoris vastus lateralis was measured during the experimental validation. The normalized muscle activity of these muscles is an outcome variable.
The motion of the orthosis with respect to the body is evaluated by means of the relative displacement between the shell and the body during a gait cycle in the sagittal plane. The relative distance was calculated from the marker positions in the sagittal plane. First, the average position of each marker frame was calculated by taking the average position of all markers of that marker frame. The rest of the steps were performed for both the upper and lower leg and their corresponding shell. Second, the translation vector from the marker frame on the leg to the marker frame on the shell was calculated by subtracting the average position of the marker frame on the leg from the average position of the marker frame on the shell. Third, the norm of this translation vector was calculated, being the distance between the marker frame on the shell and the leg. Finally, the relative displacement between the leg and the shell was

calculated by subtracting the distance between those marker frames in the static trials from this distance in a walking trial. The relative displacement during the gait cycle is an outcome variable, as is the maximum relative displacement during the gait cycle. The latter is used to compare the relative displacement between the minimal impedance mode and assistive mode trials. The correlation coefficient for the relative displacement between the minimal impedance mode and assistive mode trials is an outcome measure as well, for this same purpose.
The rotation of the orthosis with respect to the body is evaluated by means of the relative rotation between the shells and the body during a gait cycle in the sagittal plane. The relative rotation was calculated from the marker positions in the sagittal plane. First, the vector between two markers of each marker frame was calculated. Second, the vector was shifted to the origin of the global coordinate system by subtracting the position of the first marker from both markers. Third, the angle between the vector at the origin in a walking trial and the same vector in the static trial was calculated by taking the inverse tangent of the determinant of those two vectors, divided by the dot product of those two vectors. Finally, the relative rotation between the leg and the shell was calculated by subtracting the angle between the vectors of the marker frame on the leg from the angle between the vectors of the marker frame on the shell. The relative rotation during the gait cycle is an outcome measure, as is the maximum relative rotation during the gait cycle. The latter is used to compare the relative rotation between the minimal impedance mode and assistive mode trials. The correlation coefficient for the relative rotation between the minimal impedance mode and assistive mode trials is an outcome measure as well, for this same purpose.

Chapter 3

Results

The pneumatically actuated knee orthosis is evaluated based on three criteria. First the performance of the force control mechanism, in terms of force tracking error is described. Thereafter, the performance of the assistive strategy, in terms of interference with gait and muscle activity is described. Finally, the motion of the orthosis with respect to the body is described, in terms of relative displacement and relative rotation.

3.1 Force control performance

The performance of the force control is slightly better in the minimal impedance mode trials compared to the assistive mode trials (see Figures 3.1, 3.2 and 3.3). The root mean square of the force tracking error during the gait cycle is 2.10 in the minimal impedance mode trials and 2.45 in the assistive mode trials.
The force tracking error is close to 0 N during the stance phase of the gait cycle, lasting from 0 to 65% of the gait cycle. The knee joint angle stays rather constant during this phase, indicating only small movements. The root mean square of the force tracking error during the stance phase is 1.19 and 1.42 for the minimal impedance mode and assistive mode trials respectively.
During the swing phase, the absolute force tracking error increases and the knee joint angle indicates larger movements. For the minimal impedance mode and assistive mode trials, the root mean square of the force tracking error is 3.15 and 3.67 respectively.

3.2 Assistive strategy performance

The assistive strategy is evaluated in terms of interference with gait and muscle activity. To evaluate the interference with gait, the knee joint angle and gait phase duration are evaluated.

3.2.1 Gait interference

In the assistive mode trials, the assistive strategy interferes with the gait by decreasing the knee joint angle during the stance phase (see Figure 3.4). At the end of the stance phase, the knee joint angles deviates the most compared to the knee joint angle in the minimal impedance mode trials. Since the same maximum knee joint angle is reached during the swing phase for both trial types, the increase in knee joint angle at the transition from the stance phase to swing phase is larger for the assistive mode trials.
The durations of the four gait phases a gait cycle consists of are almost similar for both the minimal impedance and assistive mode trials (see Figure 3.5).

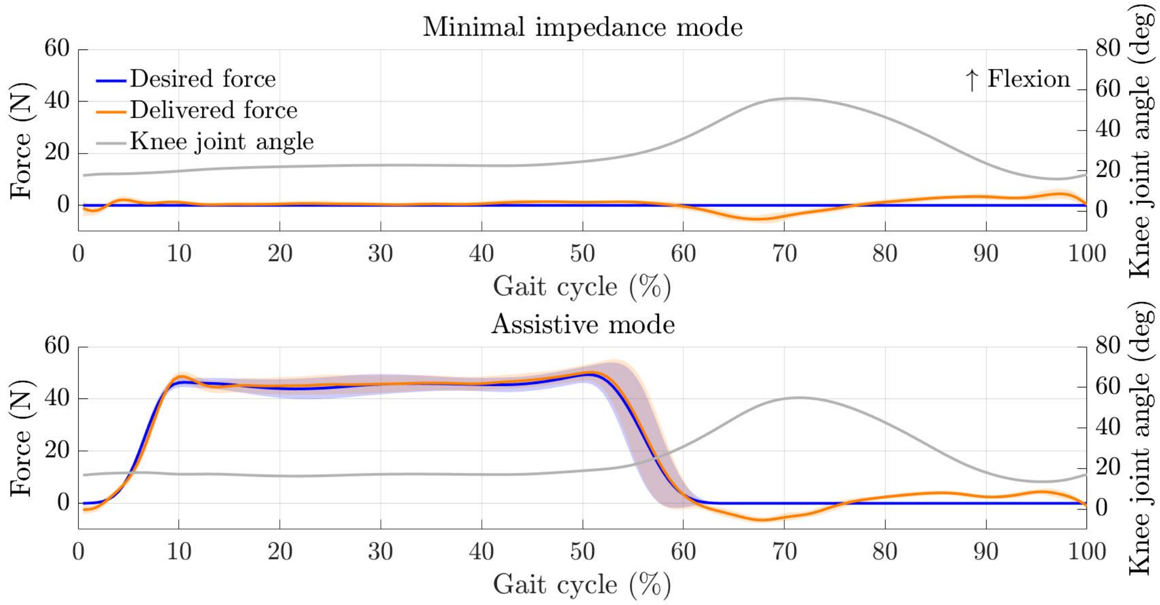

Figure 3.1: The desired force and force delivered by the orthosis during the minimal impedance mode and assistive mode trials, averaged for one subject. The shaded areas represent the standard deviation.

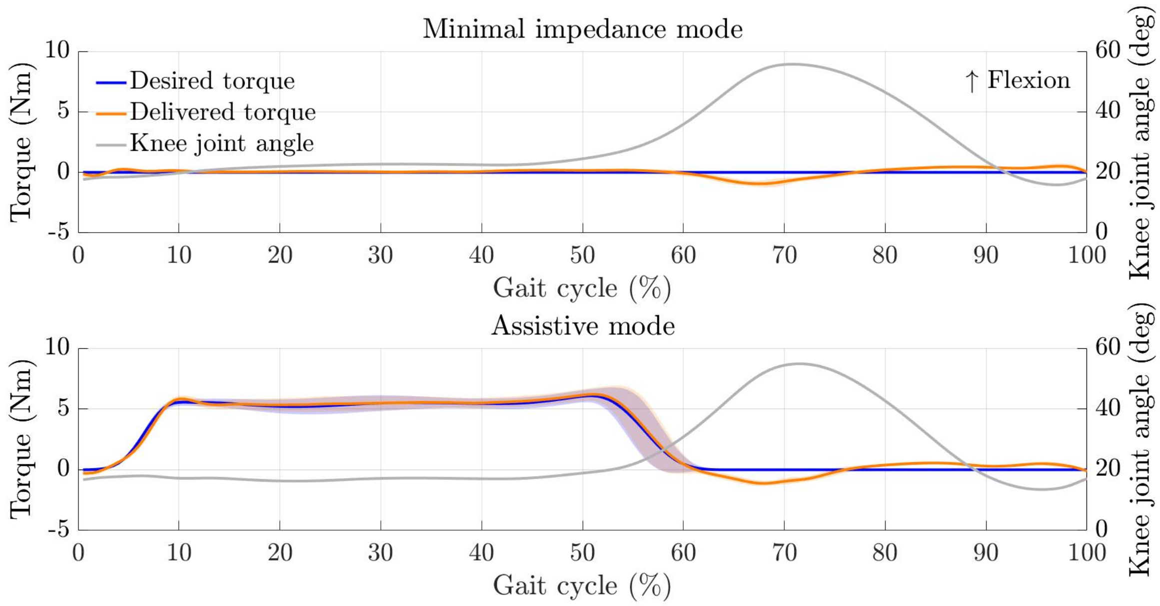

Figure 3.2: The desired torque and torque delivered by the orthosis during the minimal impedance mode and assistive mode trials, averaged for one subject. The shaded areas represent the standard deviation.

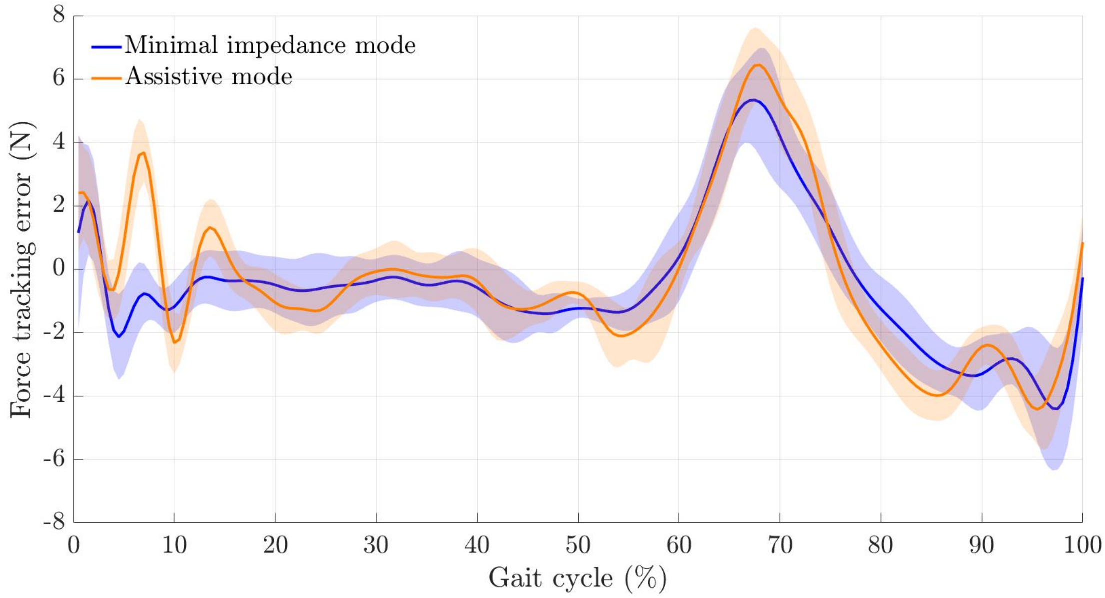

Figure 3.3: The force tracking error of the orthosis during the minimal impedance mode and assistive mode trials, averaged for one subject. The shaded areas represent the standard deviation.

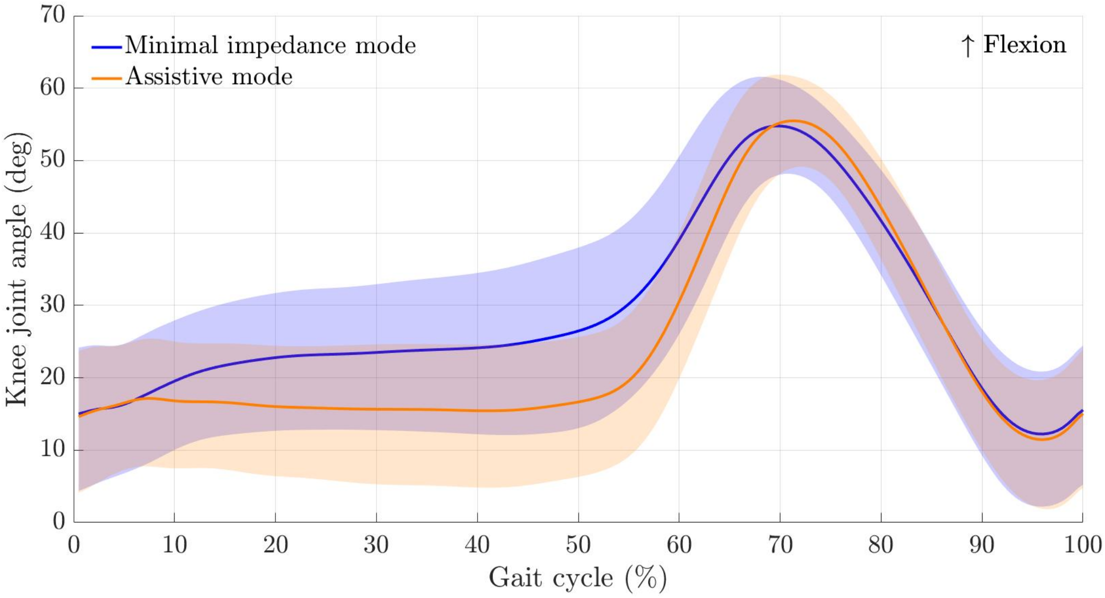

Figure 3.4: The knee joint angle during the minimal impedance mode and assistive mode trials, averaged across all subjects. The shaded areas represent the standard deviation.

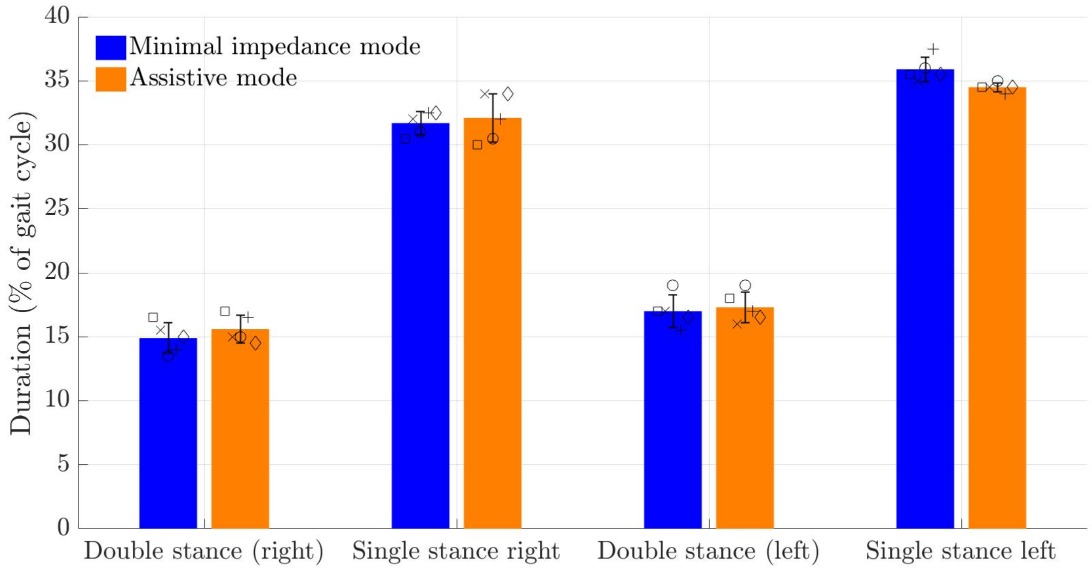

Figure 3.5: The duration of the four gait phases, as a percentage of the duration of the gait cycle, during the minimal impedance mode and assistive mode trials, averaged across all subjects. The error bars represent the standard deviation. The markers represent the durations for a single subject, each subject has its own marker.

3.2.2 Muscle activity interference

For all muscles of which the muscle activity was measured, the biceps femoris, gastrocnemius medialis, quadriceps femoris rectus femoris, and quadriceps femoris vastus lateralis, the activity was compared with literature [36, 37]. Since none of the muscle activities corresponded with literature, and can therefore not be trusted, these results are not discussed. The measured activities are shown in Appendix A.

3.3 Orthosis motion with respect to body

The motion of the orthosis with respect to the body is evaluated in terms of relative displacement and relative rotation between the shells of the orthosis and the body.

3.3.1 Relative displacement

The orthosis displaces, relative to the displacement in the static trial, with respect to the body in the minimal impedance mode and assistive mode trials (see Figures 3.6, 3.7 and 3.8). The relative displacement between the shell and the body during the gait cycle is not similar for the upper and lower shell. The maximum relative displacement is quite similar for the upper and lower shell.
In the assistive mode trials, the assistive strategy did not influence the relative displacement of the orthosis with respect to the body. The relative displacement between the shells and the body in the minimal impedance mode and assistive mode trials is strongly correlated. For the relative displacement between the upper shell and leg the correlation coefficient is 0.96, for the relative displacement between the lower shell and leg the correlation coefficient is 0.94.

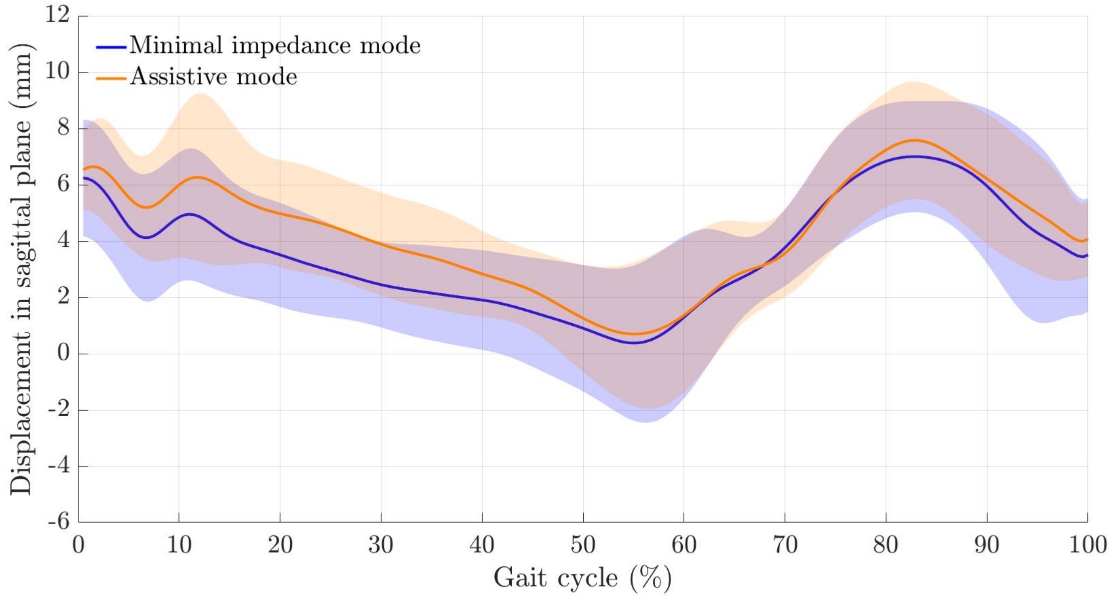

Figure 3.6: The displacement between the upper shell and the upper leg, relative to the displacement in the static trial, during the minimal impedance mode and assistive mode trials, averaged across all subjects. The shaded areas represent the standard deviation.

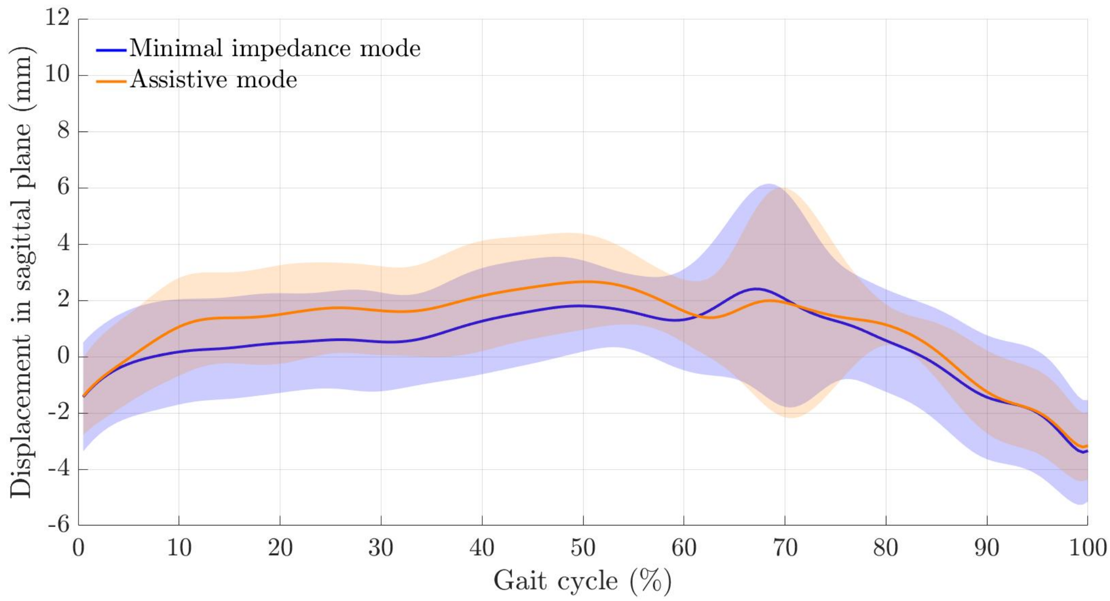

Figure 3.7: The displacement between the lower shell and the lower leg, relative to the displacement in the static trial, during the minimal impedance mode and assistive mode trials, averaged across all subjects. The shaded areas represent the standard deviation.

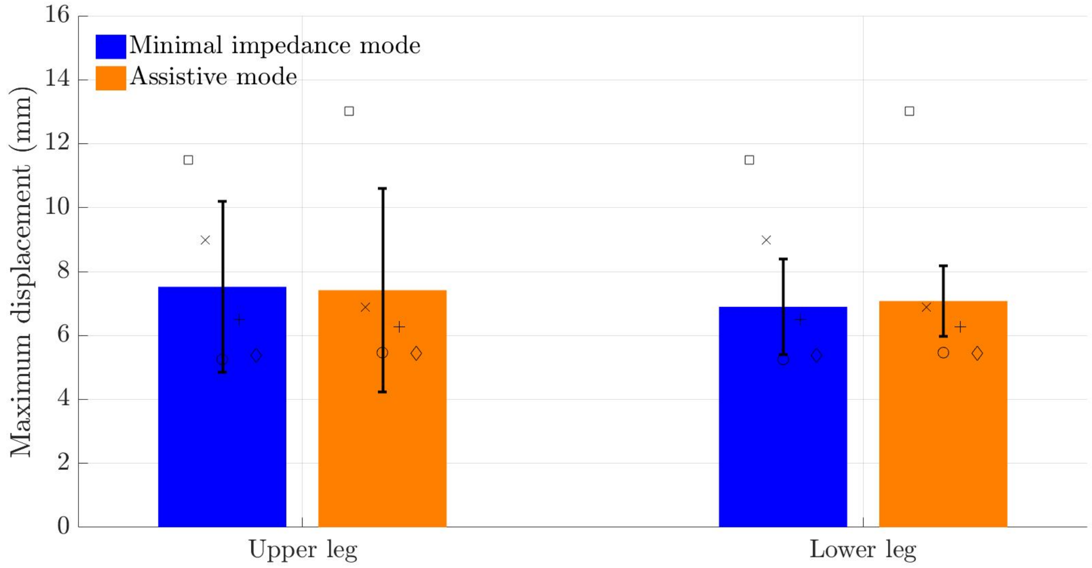

Figure 3.8: The maximum displacement between the shells and the leg, relative to the displacement in the static trial, within a gait cycle during the minimal impedance mode and assistive mode trials, averaged across all subjects. The error bars represent the standard deviation. The markers represent the maximum relative displacement for a single subject, each subject has its own marker.

3.3.2 Relative rotation

The shells of the orthosis rotate, relative to the rotation in the static trial, with respect to the body in the minimal impedance mode and assistive mode trials (see Figures 3.9, 3.10 and 3.11). The relative rotation between the shell and the body during the gait cycle is not similar of the upper and lower shell. The maximum relative rotation is quite similar for the upper and lower shell.

In the assistive mode trials, the assistive strategy did influence the relative rotation of the upper shell with respect to the body. The relative rotation between the upper shell and body in the minimal impedance mode and assistive mode trials is less similar midway during the stance phase, at around 50% of the gait cycle. The correlation coefficient for the rotation between the upper shell and leg is 0.66.

In the assistive mode trials, the assistive strategy did not influence the relative rotation of the lower shell with respect to the body. The relative rotation between the lower shell and the body in the minimal impedance mode and assistive mode trials is strongly correlated. The correlation coefficient for the rotation between the lower leg and shell is 0.96.

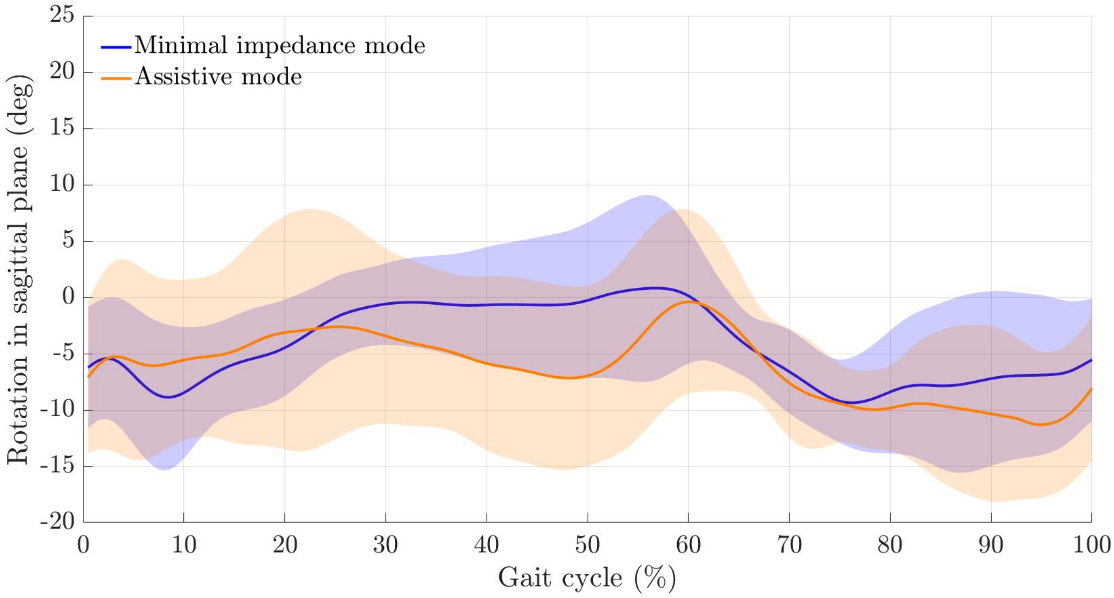

Figure 3.9: The rotation between the upper shell and the upper leg, relative to the rotation in the static trial, during the minimal impedance mode and assistive mode trials, averaged across all subjects. The shaded areas represent the standard deviation.

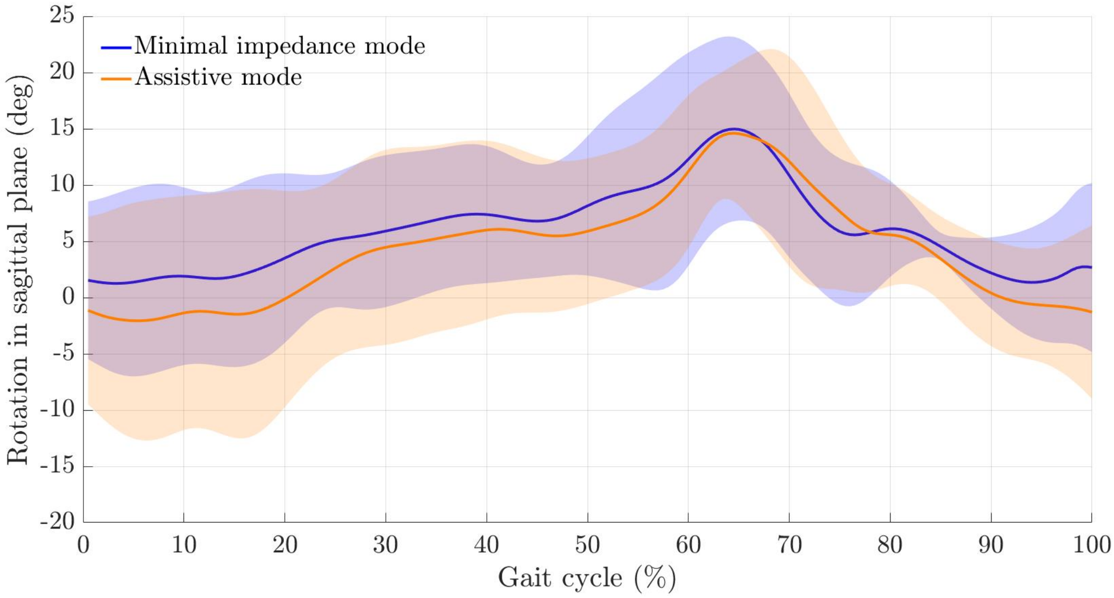

Figure 3.10: The rotation between the lower shell and the lower leg, relative to the rotation in the static trial, during the minimal impedance mode and assistive mode trials, averaged across all subjects. The shaded areas represent the standard deviation.

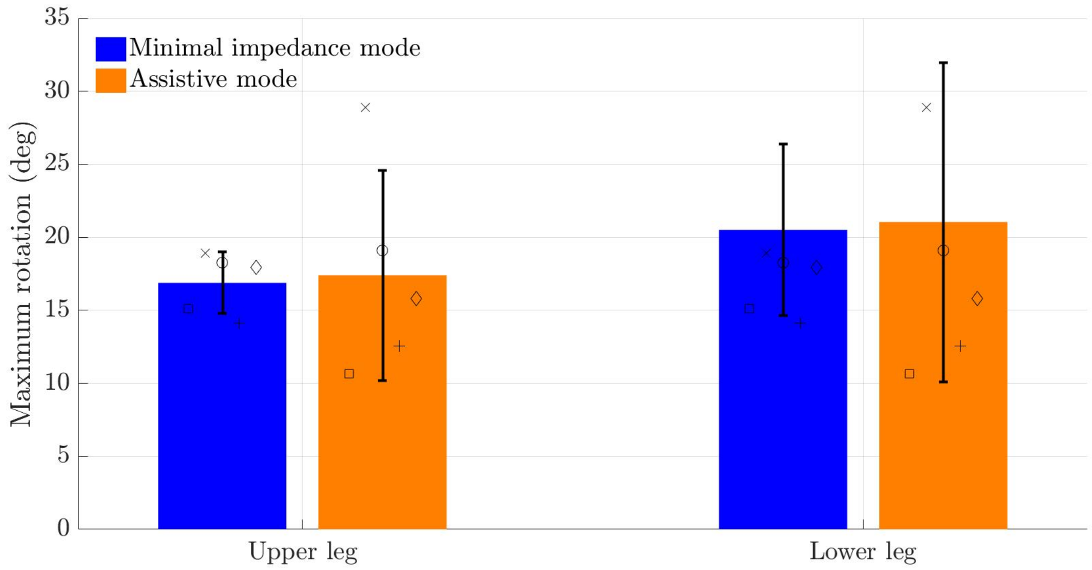

Figure 3.11: The maximum rotation between the lower shell and the lower leg, relative to the rotation in the static trial, within a gait cycle during the minimal impedance mode and assistive mode trials, averaged across all subjects. The error bars represent the standard deviation. The markers represent the maximum rotation for a single subject, each subject has its own marker.

Chapter 4

Discussion

The purpose of this study is to evaluate the pneumatically actuated knee orthosis during treadmill walking. This chapter discusses the design of the orthosis, its force control mechanism, and its assistive strategy, as well as the results obtained in the experimental validation.

The force control mechanism performed well during the experimental validation in terms of the force tracking error. Smaller force tracking errors were observed during the minimal impedance mode trails compared to the assistive mode trials.
The assistive strategy performed well during the experimental validation in terms of gait interference. The gait phase duration during the gait cycle and knee joint angle during the swing phase were not altered by the delivered assistive force. The knee joint angle during the stance phase was altered by the delivered assistive force, as the assistive strategy was designed to do. In terms of interference of the muscle activity in the upper and lower leg, the performance of the assistive strategy could not be determined. None of the measured activities in the minimal impedance mode trials matched patterns found in literature.
The orthosis moved with respect to the body during the experimental validation in terms of relative displacement and relative rotation. The relative displacement and relative rotation were different for both shells. Similar relative displacements during the gait cycle for both the minimal impedance mode and assistive mode trials were observed. The relative rotation during the gait cycle in the assistive mode trials deviated from the relative rotation in the minimal impedance mode trials. The maximum relative displacement and maximum relative rotation were similar for both the minimal impedance mode and assistive mode trials.

4.1 Force control mechanism contains assumptions

Deviations between the estimated and actual value of constants, as well as effects from neglected terms and incorrect assumptions, may have decreased the performance of the force control mechanism. By conducting experiments to find values for the constants, create expressions for the neglected terms, and confirm assumptions, or update them if needed, the performance of the force control mechanism could be improved. For several neglected terms, estimated constants, and assumptions, experiments to get more accurate estimates and expressions and to confirm the assumptions are described.
First, experiments could be performed to obtain values and expressions for unknown terms and to confirm assumptions in the mathematical model of the pneumatic cylinder [27]. These experiments should be performed with a cylinder equal to the cylinders in the orthosis. This would allow to obtain expressions for the Coulomb friction and leakage between chambers, find values for the discharge coefficient and the inactive volume of the cylinder chambers and confirm the assumption of fully laminar flow through the tubes. With these terms and constants, the mathematical model would represent the reality more closely, which could improve the performance

of the force control mechanism of the orthosis.
Second, by dismantling a valve, equal to the valve used in the orthosis, the maximum valve opening area, and its shape, could be determined. Possibly the relation between the setpoint voltage and the spool position could be determined as well. With this relation representing the reality more closely, the output of the force control mechanism could be converted to the input of the orthosis more accurate, which could improve the performance of the force control mechanism of the orthosis.
Finally, by performing an experiment in which the desired forces and movement from the actual experimental validation are mimicked, estimates for the admissible force error and the maximum valve area for the proportional term in the force control mechanism could be improved. This experiment should be performed last, since changing other factors in the force control mechanism thereafter could result in different optimum values for the estimated constants. The constants with which the smallest force tracking error was obtained during this experiment, should be used in the actual experimental validation to improve the performance of the force control mechanism of the orthosis.

4.2 Force control performance decreases for increasing desired force

The performance of the force control mechanism is likely to decrease for larger desired forces. During the minimal impedance mode trials, where the desired force was always 0 N, the performance was better compared to the assistive mode trials, where the desired force ranged between 0 and roughly 50 N. Therefore, increasing the range of the desired force even further is likely to decrease the performance of the force control mechanism. In [28], the performance of the force control mechanism was evaluated with a desired force up to 75 N. This is an indication that the force control mechanism used in this orthosis would still perform well for desired forces up to 75 N, which is a desirable feature of the force control mechanism.

4.3 Assistive strategy contains assumptions

The performance of the assistive strategy could be decreased by deviations between estimated and actual values and the neglection of terms. First, the neglection of the time derivative of the desired force in the sliding mode equation could have decreased the performance of the assistive strategy. This term could be calculated and incorporated in the sliding mode equation. Second, the calculation of the knee joint angle, used in the assistive strategy, assumes that both shells are at a similar distance from the knee joint, while this was not the case during any of the conducted experiments. The incorrect assumption of the shell placement could explain the large standard deviation observed for the knee joint angle, averaged across all subjects. If the shells are placed closer together than desired, the piston position becomes smaller, causing the knee joint angle to be larger during the entire gait cycle and the other way around.
Several factors contributed to the invalid assumption of the lengths in the knee joint angle calculation. First, the circumference of the upper and lower leg are different, invalidating the assumption that the perpendicular distance d from the segment axis to the posterior side of the segment is equal for the upper and lower leg (see Figure 2.6a) [38]. Second, the guidelines on the shell placement did not enforce the shells to be placed at the correct distance from the knee joint angle. The upper shell was supposed to be attached to the upper leg with the end of the cylinders horizontally aligned with the knee joint. However, it was not stated at what angle between the cylinders and the upper leg the shell should be positioned. For the lower

shell, there were no guidelines for its placement on the lower leg. These guidelines invalidate the assumption that the distance h from the knee joint axis to the attachment of the cylinder, parallel to the segment axis is equal for the upper and lower leg (see Figure 2.6a). A simulation of the effect of changes in d and h on the knee joint angle, desired torque, and desired force, is described in Appendix B.

The desired distance h from the knee joint axis to the attachment of the cylinder could be verified, while attaching the orthosis to the leg, to decrease the deviation between the estimated and actual distance. However, measuring this distance is not straight forward, as the distance is defined along the segment axis. It also does not account for the deviation between the assumed and actual distance d from the segment axis to the posterior side of the leg. Finally the shape of the lower shell could prevent it from being placed at the correct position, since it only fits around the lower leg in a small area.

Instead of verifying the shells are at the desired position, the distances used in the calculation of the knee joint angle could be separated for the upper and lower shell and made subject-specific. The distances can be measured after placement of the shells to get a separate value for d and h for the upper and lower shell for that subject. These four values should be entered as subject-specific constants in the knee joint angle calculation. This approach would allow more freedom in finding a tight fit between the shells and the leg. However, there are limitations in the positioning of the shells as the orthosis should not obstruct during walking. Also, measurements still have to be conducted, which are prone to errors themselves since the distances should be measured along or perpendicular to the segment axis.

4.4 Assistive strategy interferes with gait

In the assistive mode trials, the assistive strategy decreased the knee joint angle during the stance phase as designed. The assistive force delivered by the orthosis during the stance phase pushed the shells out and forward, causing the knee joint to extend. During the swing phase, the knee joint angle corresponds with the angle during the trials with the orthosis in minimal impedance mode, which is a desirable feature of the assistive strategy.

An undesirable feature of the assistive strategy is the larger knee joint angle to overcome to start the swing phase. The knee joint angle is smaller during the stance phase of the assistive mode trials compared to the minimal impedance mode trials. However, the same knee joint angle has to be reached during the swing phase. This would require more muscle activity compared to the minimal impedance mode trials, therefore requiring more muscle activity to break even before decreasing the muscle activity needed during walking.

To prevent the need for additional muscle activity to overcome a larger knee joint angle to start the swing phase, the assistance during the stance phase could be decreased earlier. This would allow the wearer to start flexing the knee at the end of the stance phase to have a smaller knee joint angle to overcome to start the swing phase. To maintain as much of the extension assistance during the stance phase, but still decrease the knee joint angle to overcome to start the swing phase, a flexion torque could be provided at the end of the stance phase. However, this could alter the knee joint angle at the end of the stance phase, since the knee joint is forced to increase faster compared to without assistance provided by the orthosis. Besides that, the orthosis is not designed to provide flexion assistance.

4.5 Orthosis does not interfere with gait

The interference with gait for wearing the orthosis itself is not part of the outcome variables of this study, since the orthosis developed in [11] was used without any alterations. However, from the results obtained during the experimental validation, it was found that wearing the orthosis in minimal impedance mode does not interfere with gait, which is a desirable feature

of the orthosis. The measured knee joint angle at a walking speed of 2 km/h corresponds with literature [39]. The gait phase durations for that same walking speed corresponds with literature as well [40].
This lack of interference with gait is beneficial for this experimental validation, since part of the goal was to investigate the interference with gait of the assistive strategy. Since the orthosis does not interfere with gait, all deviations in gait parameters found in the assistive mode trials are due to the assistive strategy.

4.6 Delivered torque deviates from required torque

The assistive torque delivered by the orthosis during the experimental validation does not correspond with the torque needed during walking in shape and magnitude. The torque needed during walking ranged from -15 to 45 Nm during the stance phase and was around -10 Nm during the swing phase [41]. The torque delivered by the orthosis was about 5 Nm during the stance phase, and 0 Nm during the swing phase. At the start and end of the stance phase, the orthosis only accounts for roughly 15% of the torque needed to walk. Midway during the stance phase, the assistive strategy even counteracts the torque exerted by the body to walk, since a flexion torque is desired but an extension torque is delivered by the orthosis. This deviation between required and delivered torque is an undesirable feature of the assistive strategy.
The force that can be delivered by the orthosis is not a limiting factor in the assistive strategy. The two cylinders can deliver an extension torque of 1000 N when the pressure in chamber 1 of the cylinders is equal to the supply pressure and the pressure in chamber 2 of the cylinders is equal to the atmospheric pressure (see Equation 2.1). During the stance phase, with a lever arm of 120 mm, this would result in a knee joint torque of 120 Nm. In the middle of the swing phase, with a lever arm of 180 mm, this would result in a knee joint torque of 180 Nm. These torques exceed the torque needed during walking, which is a desirable feature of the orthosis.
Increasing the magnitude of the assistive torque will not improve the performance of the assistive strategy. It would give more assistance at the start and end of the stance phase, which is desirable. However, midway during the stance phase, the assistance would counteract the desired flexion torque even more, which is undesirable. Besides that, higher torques delivered by the orthosis were described as uncomfortable. This was investigated during a preliminary experiment with one subject to find the correct parameters for the assistive strategy.
By letting the assistive strategy mimick the torque needed during walking more closely, the benefit the wearer gets from the delivered torque could increase. For when extension torques are needed to walk, the assistive strategy should mimick this pattern. By providing part of the torque needed to walk, the muscle activity needed to walk could decrease. Since the orthosis is designed to deliver only compressional forces, the assistive strategy should deliver zero torque if a flexion torque is needed during walking. This does not mimick the pattern, but at least does not counteract the wearer.

4.7 Orthosis influences measurements of muscle activity

The placement of the surface electrodes to measure the muscle activity was limited by the design of the orthosis. The shells contained cutouts to place the surface electrodes for the biceps femoris and gastrocnemius medialis on the posterior side of the leg (see Figure 4.1). However, it is possible that the optimal location was beneath the shell instead of within a cutout. The optimal surface electrode locations for the quadriceps femoris rectus femoris and quadriceps femoris vastus lateralis, located at the anterior side of the leg, were less restricted by the orthosis. However, it is still possible that one of the straps crossed the ideal location. These restrictions on surface electrode placement are an undesirable feature of the orthosis.
These limitations could explain the lack of correspondence with muscle activities found in liter-

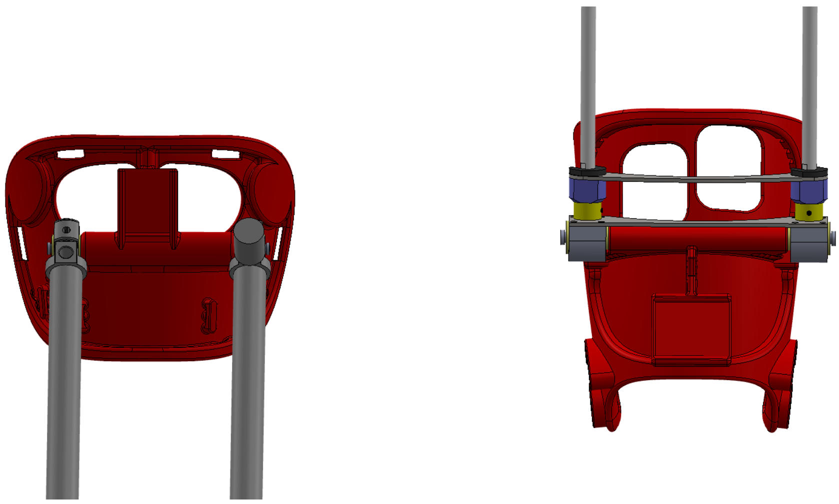

Figure 4.1: Drawings of the upper (left) and lower (right) shells of the pneumatically actuated knee orthosis, viewed from the posterior side. The two large cutouts in each shell leave room to place surface electrodes.

ature [36, 37]. First, the surface electrodes were placed on less ideal locations if the shells or the straps covered the optimal location. As a result, the amplitude of the measured signal could be less and the measurement could contain artifacts from other nearby muscles. Second, movement of the orthosis during walking could deform the skin around the straps and shells. This could cause artifacts in the muscle activity measurements as well, since the location of the sensor with respect to the muscle may change.

To overcome these limitations regarding the placement of surface electrodes, the surface that the shells and the straps cover could be reduced. However, this would decrease the area on which the force delivered by the orthosis is transferred to the body, resulting in more discomfort for the wearer. The amount of surface of the shell that could be removed is limited, as the cylinders and the Boa closure systems need to stay connected to the shells. The cables from the Boa closure system are already thin and cause some discomfort for the wearer as they press into the leg, which leaves no room for reducing the area they cover. The velcro straps wrapping around the anterior side of the leg are wider, but apply more force on the leg as well. Making these straps smaller, would lead to more discomfort for the wearer.

Another improvement that would allow better surface electrode placement is to concentrate the surface that the shells and straps cover to the lateral and medial sides of the leg, where no surface electrodes have to be placed. However, this would require a redesign of the complete orthosis, since the attachment points of the orthosis and the Boa closure systems would have to be moved as well to maintain a tight fit with the body. With this decision it has to be kept in mind that the goal of the orthosis is to deliver assistance during walking. To do so, the measured muscle activity is not needed. It is only measured to validate the assistance provided by the orthosis.

Instead of altering the orthosis, the way to evaluate the performance of its assistive strategy could be adjusted as well. The subjects stated that they could feel that the orthosis provided assistance after the assistive mode was disabled at the end of a trial more than they could feel the assistance during walking. They felt as if they would fall to their knees the first time the right leg would strike the treadmill. Given this observation, the performance of the assistive strategy may be evaluated using two gait parameters, the knee joint angle and the gait phase duration, after disabling the assistive mode. These gait parameters were already evaluated in this experimental validation, but only with the orthosis in either minimal impedance mode or assistive mode. The data collection ended before changing the mode of the orthosis. If those gait parameters deviate from the gait parameters with the assistive mode of the orthosis enabled, it is an indication that the assistive strategy interferes with gait or vice versa.

4.8 Orthosis allows for motion with respect to body

The relative displacement and relative rotation observed between the shells and the body during walking could be explained by motion of the orthosis with respect to the body. First, this could be the result of the orthosis not being attached firmly enough for the shells to stay in place during walking. It was not always possible to get a tight fit between the shells and the leg. Besides that, the securing of the straps had to be redone during the experimental validation sometimes and it felt uncomfortable for the wearer to have the straps secured tightly. Another explanation for the motion between the shells and the body could be that the arrangement of the straps allows for motion, or that there are just not enough straps to restrict motion in all directions. This movement with respect to the body is an undesirable feature of the orthosis.

The relative displacement with respect to the body observed in this study is within the range of relative displacement found in other studies, which is a desirable feature of the orthosis. In [24], the relative displacement of the pelvis and thigh cuff with respect to the body was 3.1 $\pm$ 2.0 mm and 4.0 $\pm$ 0.6 mm respectively with the assistive device not delivering assistive force. In [25], larger relative displacements with respect to the body were observed, namely between 6.1 mm and 25.4 mm with a mean of 12 mm for the left knee position and between 2.7 mm and 19.5 mm with a mean of 10.3 mm for the right knee position. In some other studies which investigated the motion of the assistive device with respect to the body while standing up and sitting down, relative displacements of up to 40 mm were observed [42, 43]. The magnitude of relative displacement is lower than 11.7 mm, which was found to not result in any observed damage to the skin or reported pain on the fore arm [44].

The relative rotation with respect to the body observed in this study is larger compared to relative rotations found in literature, which is an undesirable feature of the orthosis. In [24], rotation of the thigh link with respect to the body of around 10 degrees was found with during standing up and sitting down. The rotations contributed to an uneven distribution of slippage beneath the cuff and large relative displacements, which indicated a high risk of injuries.

Slippage of the orthosis with respect to the body may not be the cause of the observed relative displacement. In [43], relative displacements of around 20 mm were observed during standing up and sitting down. These relative displacements were stated to be too large to be due to skin deformation only. Slippage of the cuff during that experimental validation was stated as a possible explanation for the high relative displacement [43]. In [42], relative displacements of around 40 mm were observed during standing up and sitting down. Slippage was measured as well, but with a magnitude of only several millimeters. The observed relative displacement, after subtracting slippage, was stated to be too high to be the result of skin stretching alone. The probable cause for the high relative displacement was stated to be deformation of skin, fat and muscle tissues [42]. The observed relative displacements in these studies are smaller compared to the observed relative displacements in this study. This could be an indication that the observed relative displacements are due to skin, fat, and/or tissue deformation.

The fact that the relative displacement during the gait cycle, and the maximum relative displacement and relative rotation were similar for both trial types could indicate that the observed motion was indeed the result of deformation of the leg. There are no measurements available of the position of the markers on the body with respect to fixed point on that same body part. With this data, any movement due to deformation of the leg could be calculated and compensated for while analyzing the data. By adding markers on bony landmarks, the lateral epicondyle and malleolus for example, the relative displacement between the markers on the body with respect to the bony landmark of that body part could be calculated. However, soft tissue artifacts are present on these bony landmarks as well [45].

To decrease the amount of motion, a redesign of the entire orthosis is needed. The shape and size of the shells, as well as the mesh of straps used to attach the orthosis to the body should be considered when improving the design.

4.9 Assistive strategy does not interfere with relative displacement

The assistive strategy did not interfere with the relative displacement of the shells with respect to the body. The maximum relative displacement and the relative displacement during the gait cycle are the same for both the minimal impedance mode and assistive mode trials. In [24], a positive trend in the relative displacement between cuffs and the body was observed that is related to the increment of delivered assistance. In [43], different interaction forces between the cuffs and the body were found when comparing trials with and without provided assistance. This robustness for changes in provided assistance, in terms of relative displacement of the orthosis with respect to the body, is a desirable feature of the orthosis.

4.10 Assistive strategy interferes with relative rotation

The assistive strategy did interfere with the relative rotation of the orthosis with respect to the body during the gait cycle. The relative rotation of the upper shell during the gait cycle around the middle of the stance phase during the assistive mode trials deviates from the relative rotation during the minimal impedance mode trials. This interference in the relative rotation of the orthosis with respect to the body, is an undesirable effect of the design of the orthosis.

The relative rotation of the lower shell during the gait cycle is the same for both the minimal impedance mode and assistive mode trials. This robustness for changes in provided assistance, in terms of relative rotation of the lower shell with respect to the body, is a desirable feature of the orthosis.

The interference with the relative rotation of the shells during the middle part of the stance phase could be explained by the assistive force that was delivered during that period. Part of the delivered force resulted in a smaller knee joint angle, as the assistive strategy was designed to do (see Figure 3.4). However, part of the delivered force may have resulted in rotating the shell with respect to the leg, instead of extending the knee. This relative rotation of the shell instead of extension of the knee could be due to resistance of the wearer to deviate from normal gait. Even though some deviation from normal gait is observed, the wearer might counteract the assistive force of the orthosis when the deviation becomes too large.

The increased relative rotation of the upper shell with respect to the body may be an explanation for the subject who participated in the preliminary experiment to feel uncomfortable when a higher assistive force was delivered by the orthosis. The surface of the shell through which the force delivered by the orthosis was transferred to the body decreases when it rotates. Therefore, the same amount of force is transferred on a smaller area. At the same time, the shear forces that may be present between the shell and the body will be present on a smaller area as well. Therefore, the threshold for the shear forces to be uncomfortable to the wearer will be reached sooner if the shell is rotated and the contact area is smaller.

The assistive strategy did not interfere with the maximum relative rotation of the shells with respect to the body. The maximum relative rotation is the same for both the minimal impedance mode and assistive mode trials. This robustness for changes in provided assistance, in terms of maximum relative rotation of the orthosis with respect to the body, is a desirable feature of the orthosis.

Chapter 5

Conclusion

This chapter summarizes the findings regarding the evaluation of the pneumatically actuated knee orthosis. Thereafter, recommendations for further research are presented.

This study evaluated the pneumatically actuated knee orthosis based on the performance of the force control mechanism, the performance of the assistive strategy and the motion of the orthosis with respect to the body in terms of relative displacement and relative rotation.
The performance of the force control mechanism was good during the experimental validation. The performance was slightly better for the orthosis in minimal impedance mode compared to the orthosis in assistive mode. The performance was better during the swing phase compared to the stance phase, independent of the mode of the orthosis.
The assistive strategy performed well in terms of interference with gait. There was no interference with the knee joint angle and gait phase duration, other than the intended effect on the knee joint angle during the stance phase. It could not be concluded if the assistive strategy decreased the muscle activity during walking, due to incorrect muscle activity measurements.
The design of the orthosis allowed for relative displacement and relative rotation with respect to the body, which is not desirable. Providing assistance did not interfere with the relative displacement, but did interfere with the relative rotation.
Further research can be done on finding a suitable assistive strategy to assist the wearer during walking. The current assistive strategy interferes with the knee joint angle, counteracts the wearer midway during the stance phase, and provides roughly 15% of the torque required during walking. With these insights, a more suitable assistive strategy could be designed.
Besides that, further research can be done on finding a suitable way of validating the effectiveness of the assistive strategy. It is possible that with accurate placement of the orthosis and the surface electrodes, reliable muscle activity measurements could be performed. Another option could be to validate the effectiveness of the assistive strategy by means of other measures, such as gait parameters after disabling the assistance.

References

[1] Aaron M Dollar and Hugh Herr. Lower extremity exoskeletons and active orthoses: challenges and state-of-the-art. *IEEE Transactions on Robotics*, 24(1):144–158, 2008.

[2] Khairul Anam and Adel Ali Al-Jumaily. Active exoskeleton control systems: state of the art. *Procedia Engineering*, 41:988–994, 2012.

[3] Alan T Asbeck, Stefano MM De Rossi, Ignacio Galiana, Ye Ding, and Conor J Walsh. Stronger, smarter, softer: next-generation wearable robots. *IEEE Robotics & Automation Magazine*, 21(4):22–33, 2014.

[4] George L Cobb. Walking motion, August 6 1935. US Patent 2,010,482.

[5] John H Murphy. Leg brace, November 6 1951. US Patent 2,573,866.

[6] ND Jaukovic. Active peroneal orthosis. In *Proceedings of the International Symposium on External Control of Human Extremities*, pages 13–20, 1981.

[7] Joaquin A Blaya and Hugh Herr. Adaptive control of a variable-impedance ankle-foot orthosis to assist drop-foot gait. *IEEE Transactions on Neural Systems and Rehabilitation Engineering*, 12(1):24–31, 2004.

[8] Daniel P Ferris, Joseph M Czerniecki, and Blake Hannaford. An ankle-foot orthosis powered by artificial pneumatic muscles. *Journal of Applied Biomechanics*, 21(2):189–197, 2005.

[9] Michael Wehner, Brendan Quinlivan, Patrick M Aubin, Ernesto Martinez-Villalpando, Michael Baumann, Leia Stirling, Kenneth Holt, Robert Wood, and Conor Walsh. A lightweight soft exosuit for gait assistance. In *2013 IEEE International Conference on Robotics and Automation (ICRA)*, pages 3362–3369. IEEE, 2013.

[10] Alan T Asbeck, Stefano MM De Rossi, Kenneth G Holt, and Conor J Walsh. A biologically inspired soft exosuit for walking assistance. *The International Journal of Robotics Research*, 34(6):744–762, 2015.

[11] Martijn E Grootens, Edsko EG Hekman, and Herman van der Kooij. The inverted muscle skeleton approach: moving beyond rigid exoskeletons. In *2018 7th IEEE International Conference on Biomedical Robotics and Biomechatronics (BioRob)*, pages 659–664. IEEE, 2018.

[12] Jose L Pons. Rehabilitation exoskeletal robotics. *IEEE Engineering in Medicine and Biology Magazine*, 29(3):57–63, 2010.

[13] Bing Chen, Hao Ma, Lai-Yin Qin, Fei Gao, Kai-Ming Chan, Sheung-Wai Law, Ling Qin, and Wei-Hsin Liao. Recent developments and challenges of lower extremity exoskeletons. *Journal of Orthopaedic Translation*, 5:26–37, 2016.

[14] Bing Chen, Bin Zi, Zhengyu Wang, Ling Qin, and Wei-Hsin Liao. Knee exoskeletons for gait rehabilitation and human performance augmentation: a state-of-the-art. *Mechanism and Machine Theory*, 134:499–511, 2019.

[15] Jinghui Cao, Sheng Quan Xie, Raj Das, and Guo L Zhu. Control strategies for effective robot assisted gait rehabilitation: the state of art and future prospects. *Medical Engineering & Physics*, 36(12):1555–1566, 2014.

[16] Gery Colombo, Matthias Joerg, Reinhard Schreier, Volker Dietz, et al. Treadmill training of paraplegic patients using a robotic orthosis. *Journal of Rehabilitation Research and Development*, 37(6):693–700, 2000.

[17] Hao Ma, Wai-Yin Lai, Wei-Hsin Liao, Daniel Tik-Pui Fong, and Kai-Ming Chan. Design and control of a powered knee orthosis for gait assistance. In *2013 IEEE/ASME International Conference on Advanced Intelligent Mechatronics*, pages 816–821. IEEE, 2013.

[18] Jung-Hoon Kim, Myounghoon Shim, Dong Hyun Ahn, Byoung Jong Son, Suk-Young Kim, Deog Young Kim, Yoon Su Baek, and Baek-Kyu Cho. Design of a knee exoskeleton using foot pressure and knee torque sensors. *International Journal of Advanced Robotic Systems*, 12(8):112, 2015.

[19] Alexander Duschau-Wicke, Joachim Von Zitzewitz, Andrea Caprez, Lars Lünenburger, and Robert Riener. Path control: a method for patient-cooperative robot-aided gait rehabilitation. *IEEE Transactions on Neural Systems and Rehabilitation Engineering*, 18(1):38–48, 2009.

[20] Michael S Cherry, Sridhar Kota, Aaron Young, and Daniel P Ferris. Running with an elastic lower limb exoskeleton. *Journal of Applied Biomechanics*, 32(3):269–277, 2016.

[21] Aaron J Young and Daniel P Ferris. State of the art and future directions for lower limb robotic exoskeletons. *IEEE Transactions on Neural Systems and Rehabilitation Engineering*, 25(2):171–182, 2016.

[22] Matthew B Yandell, Brendan T Quinlivan, Dmitry Popov, Conor Walsh, and Karl E Zelik. Physical interface dynamics alter how robotic exosuits augment human movement: implications for optimizing wearable assistive devices. *Journal of NeuroEngineering and Rehabilitation*, 14(1):1–11, 2017.

[23] Damiano Zanotto, Yasuhiro Akiyama, Paul Stegall, and Sunil K Agrawal. Knee joint misalignment in exoskeletons for the lower extremities: effects on user's gait. *IEEE Transactions on Robotics*, 31(4):978–987, 2015.

[24] Nicolò d'Elia, Federica Vanetti, Marco Cempini, Guido Pasquini, Andrea Parri, Marco Rabuffetti, Maurizio Ferrarin, Raffaele Molino Lova, and Nicola Vitiello. Physical human-robot interaction of an active pelvis orthosis: toward ergonomic assessment of wearable robots. *Journal of NeuroEngineering and Rehabilitation*, 14(1):1–14, 2017.

[25] N Neckel, W Wisman, and J Hidler. Limb alignment and kinematics inside a lokomat robotic orthosis. In *2006 International Conference of the IEEE Engineering in Medicine and Biology Society*, pages 2698–2701. IEEE, 2006.

[26] Kevin Langlois, Marta Moltedo, Tomislav Bacek, Carlos Rodriguez-Guerrero, Bram Vanderborght, and Dirk Lefeber. Design and development of customized physical interfaces to reduce relative motion between the user and a powered ankle foot exoskeleton. In *2018 7th IEEE International Conference on Biomedical Robotics and Biomechatronics (BioRob)*, pages 1083–1088. IEEE, 2018.

[27] Edmond Richer and Yildirim Hurmuzlu. A high performance pneumatic force actuator system: part i-nonlinear mathematical model. *Transactions-American Society of Mechanical Engineers Journal of Dynamic Systems Measurement and Control*, 122(3):416–425, 2000.

[28] Edmond Richer and Yildirim Hurmuzlu. A high performance pneumatic force actuator system: part ii-nonlinear controller design. *Transactions-American Society of Mechanical Engineers Journal of Dynamic Systems Measurement and Control*, 122(3):426–434, 2000.

[29] Festo. *Proportional directional control valves MYPE.*

[30] Yuri Shtessel, Christopher Edwards, Leonid Fridman, and Arie Levant. Introduction: intuitive theory of sliding mode control. In *Sliding Mode Control and Observation*, pages 1–42. Springer, 2014.

[31] Wilfrid Perruquetti and Jean-Pierre Barbot. *Sliding mode control in engineering.* CRC press, 2002.

[32] David A Winter. *Biomechanics and motor control of human movement.* John Wiley & Sons, 2009.

[33] MP Kadaba, HK Ramakrishnan, and ME Wootten. Measurement of lower extremity kinematics during level walking. *Journal of Orthopaedic Research*, 8(3):383–392, 1990.

[34] Recommendations for sensor locations on individual muscles. http://seniam.org/.

[35] Peter Konrad. The abc of emg. *A practical introduction to kinesiological electromyography*, 1(2005):30–5, 2005.

[36] David A Winter and HJ Yack. Emg profiles during normal human walking: stride-to-stride and inter-subject variability. *Electroencephalography and Clinical Neurophysiology*, 67(5):402–411, 1987.

[37] Yuri P Ivanenko, Richard E Poppele, and Francesco Lacquaniti. Five basic muscle activation patterns account for muscle activity during human locomotion. *The Journal of Physiology*, 556(1):267–282, 2004.

[38] Dined anthropometric database. https://dined.io.tudelft.nl/en/database/tool.

[39] Benjamin F Mentiplay, Megan Banky, Ross A Clark, Michelle B Kahn, and Gavin Williams. Lower limb angular velocity during walking at various speeds. *Gait & Posture*, 65:190–196, 2018.

[40] Felix Hebenstreit, Andreas Leibold, Sebastian Krinner, Götz Welsch, Matthias Lochmann, and Bjoern M Eskofier. Effect of walking speed on gait sub phase durations. *Human Movement Science*, 43:118–124, 2015.

[41] D Casey Kerrigan, Patrick O Riley, Tanya J Nieto, and Ugo Della Croce. Knee joint torques: a comparison between women and men during barefoot walking. *Archives of Physical Medicine and Rehabilitation*, 81(9):1162–1165, 2000.

[42] Yasuhiro Akiyama, Shogo Okamoto, Yoji Yamada, and Kenji Ishiguro. Measurement of contact behavior including slippage of cuff when using wearable physical assistant robot. *IEEE Transactions on Neural Systems and Rehabilitation Engineering*, 24(7):784–793, 2015.

[43] Yasuhiro Akiyama, Yoji Yamada, and Shogo Okamoto. Interaction forces beneath cuffs of physical assistant robots and their motion-based estimation. *Advanced Robotics*, 29(20):1315–1329, 2015.

[44] Jamaluddin Mahmud, Cathy A Holt, and Sam L Evans. An innovative application of a small-scale motion analysis technique to quantify human skin deformation in vivo. *Journal of Biomechanics*, 43(5):1002–1006, 2010.

[45] Alana Peters, Brook Galna, Morgan Sangeux, Meg Morris, and Richard Baker. Quantification of soft tissue artifact in lower limb human motion analysis: a systematic review. *Gait & Posture*, 31(1):1–8, 2010.

Appendices

A Muscle activity results

During the experimental validation, the muscle activities were measured and processed afterwards. The results, which did not correspond with literature, are shown in Figures A.1-A.4.

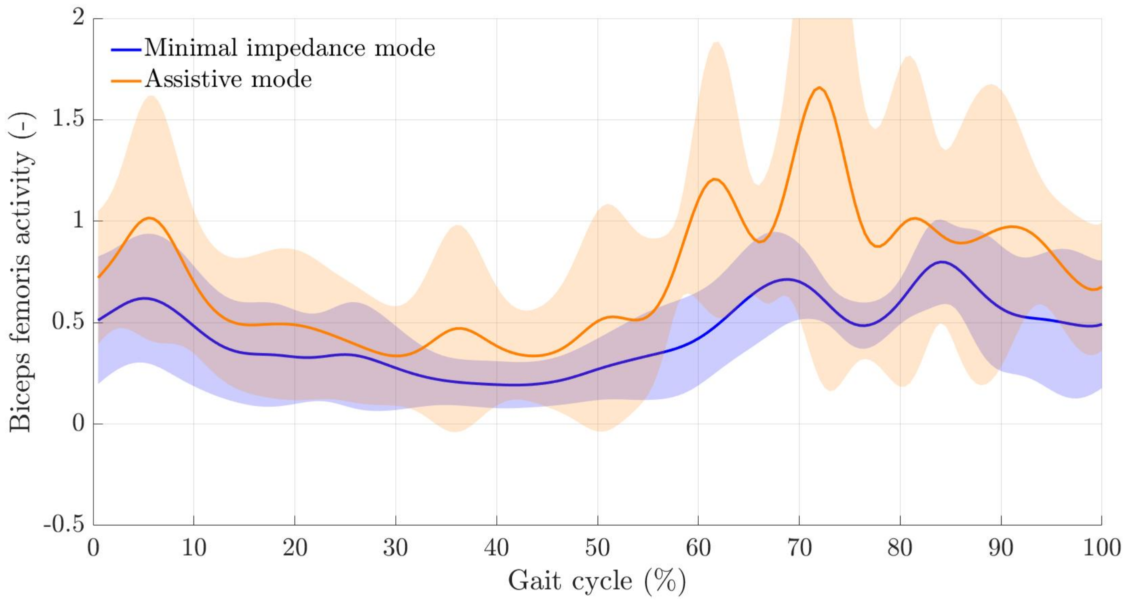

Figure A.1: The normalized muscle activity of the biceps femoris during the minimal impedance mode and assistive mode trials, averaged across all subjects. The shaded areas represent the standard deviation.

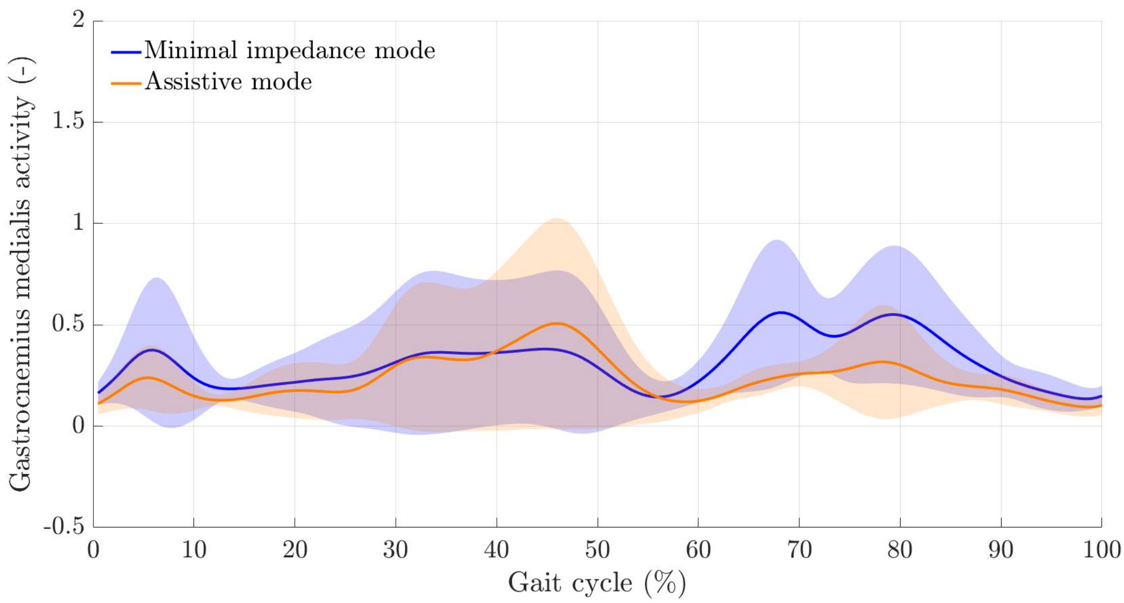

Figure A.2: The normalized muscle activity of the gastrocnemius medialis during the minimal impedance mode and assistive mode trials, averaged across all subjects. The shaded areas represent the standard deviation.

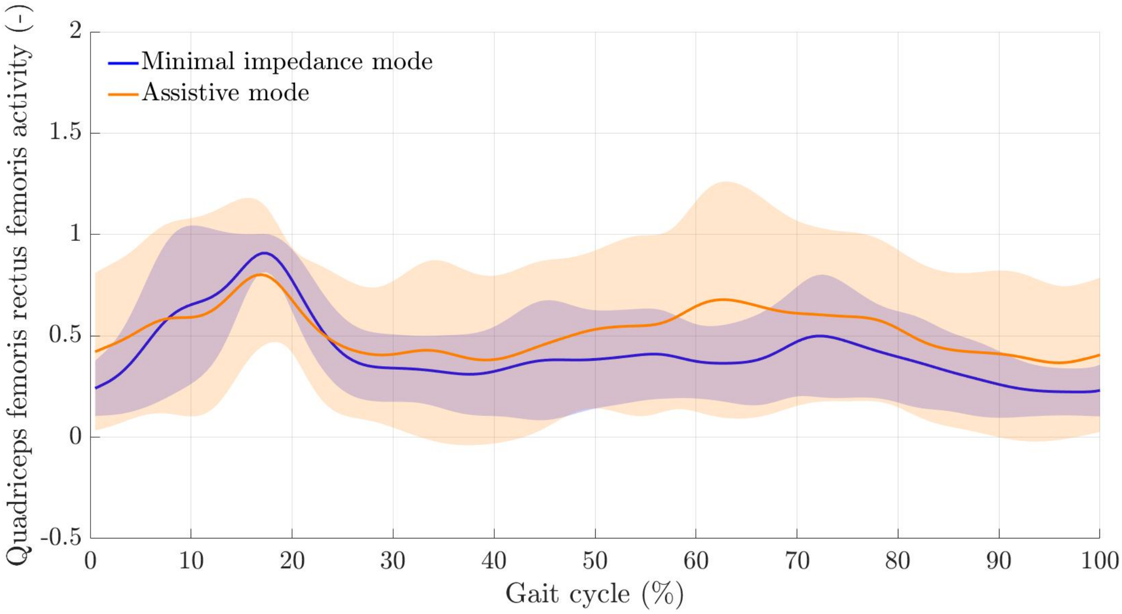

Figure A.3: The normalized muscle activity of the quadriceps femoris rectus femoris during the minimal impedance mode and assistive mode trials, averaged across all subjects. The shaded areas represent the standard deviation.

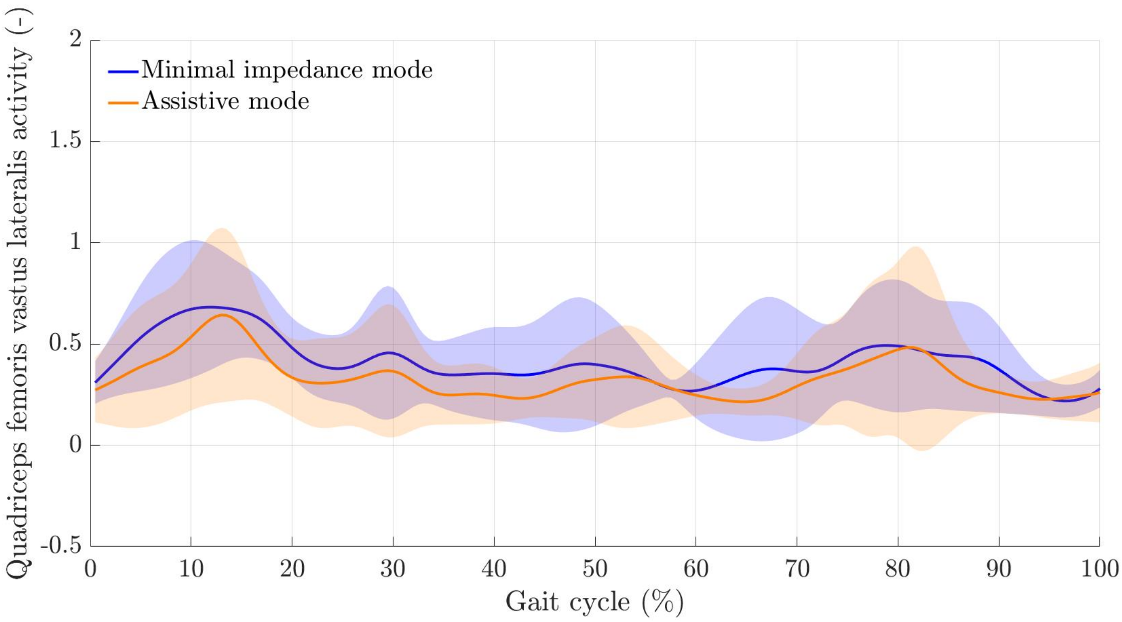

Figure A.4: The normalized muscle activity of the quadriceps femoris vastus lateralis during the minimal impedance mode and assistive mode trials, averaged across all subjects. The shaded areas represent the standard deviation.

B Simulations on knee joint angle, desired torque, and desired force

During the experimental validation, the perpendicular distance d from the segment axis to the posterior side of the segment and the distance h from the knee joint axis to the attachment of the cylinder were different compared to the estimated values. Since these distances are used in the calculation of the knee joint angle, the desired torque, and the desired force, this deviation may cause a decrease in performance of the assistive strategy, as stated in Section 4.3.
To investigate the influence of this deviation between the estimated and actual distances, some simulations were done on the knee joint angle, the desired torque, and the desired force with different values for d and h. In this appendix, the way these simulations were performed is described and the results are presented and discussed.

B.1 Method

The Simulink model used to control the orthosis calculated the knee joint angle, the desired torque, and the desired force, as described in Section 2.3. To calculate the knee joint angle, the measured piston position is used. For the calculation of the desired torque and the desired force, the piston position, the time since the start of the stance phase of the right leg, the estimated duration of this stance phase and the current gait phase are used.
To investigate the effect of d and h on the knee joint angle, the desired torque, and the desired force, these values were calculated using the functions from the Simulink model, but with altered distances d and h. For each of the values d and h have an effect on, the knee joint angle, the desired torque, and the desired force, five simulations were performed. In the first simulation, the distance for d and h was similar to the values used in the experimental validation. In the other four simulations, either the distance d or h was increased or decreased by 10%. Therefore, a total of 15 simulations was performed on the calculation of the knee joint angle, the desired torque, and the desired force.
As input values for the simulations, the processed data obtained during the experimental validation was used. Since the data was split into gait cycles during the data processing, the simulations span one gait cycle. For the simulation of the effect of d and h on the knee joint angle, the piston position during the trials with the orthosis in assistive mode, averaged across all subjects, was used. For the simulation of the effect of d and h on the desired torque and desired force, the gait phase during the trials with the orthosis in assistive mode, averaged across all subjects, was used, as well as the piston position.
The data was time-interpolated during processing to eliminate the effect of the gait cycle duration. However, since the calculation of the desired torque and the desired force is time dependent, this processed data could not be used in the simulation directly. Instead, the data was resampled to a gait cycle duration of 1.5 seconds, which was estimated after inspecting the raw data. The duration of the stance phase of the right leg was fixed to 1 second, which is 67% of the gait cycle duration. The calculated desired torque and desired force were resampled back to 200 data points per gait cycle to be able to display the values against the percentage of the gait cycle.

B.2 Results

Increasing the perpendicular distance d from the segment axis to the posterior side of the segment leads to a decrease of the knee joint angle, and vice versa (see Figure B.1). The maximum deviation is three degrees, which is observed when the knee joint angle is largest, at around 70% of the gait cycle.
Increasing the distance h from the knee joint axis to the attachment of the cylinder leads to an increase of the knee joint angle, and vice versa (see Figure B.2). The maximum deviation is 30 degrees, which is observed at the end of the swing phase of the right leg, at around 95% of the

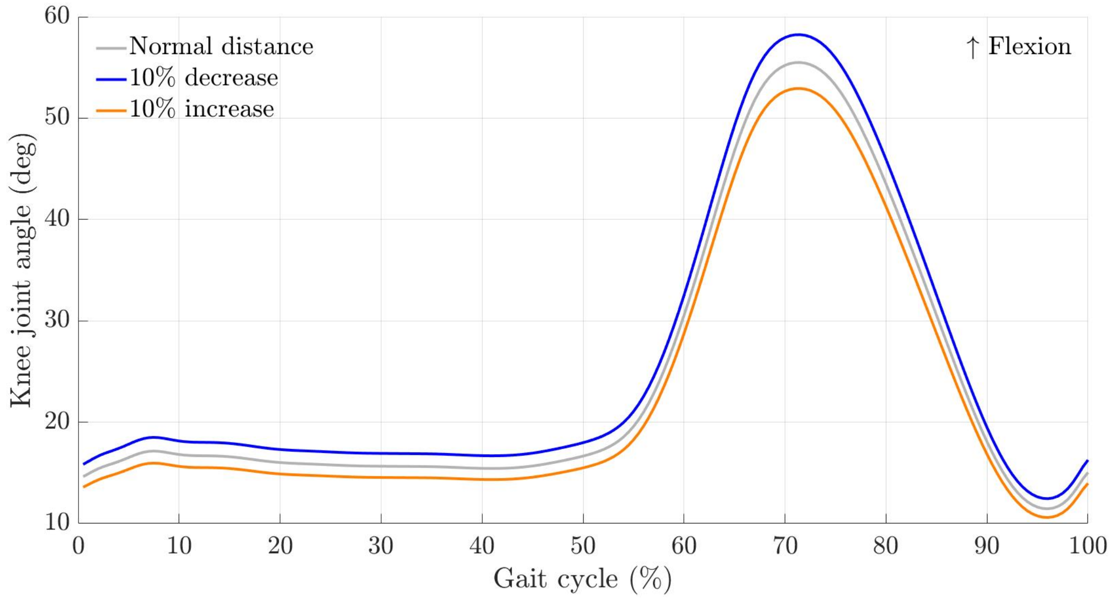

Figure B.1: The knee joint angle during minimal impedance mode trials, averaged across all subjects, and the simulated knee joint angle for a 10% decrease and increase of the perpendicular distance d from the segment axis to the posterior side of the segment.

gait cycle.
Increasing the perpendicular distance d from the segment axis to the posterior side of the segment leads to a decrease of the desired torque and desired force, and vice versa (see Figures B.3 and B.4). The maximum deviation in desired torque and desired force are 0.25 Nm and 2.5 N respectively, which are observed during the stance phase, from around 10 to 50% of the gait cycle.
Increasing the distance h from the knee joint axis to the attachment of the cylinder leads to an increase of the desired torque and desired force, and vice versa (see Figure B.5). The maximum deviation in torque and force are 3.5 Nm and 30 N respectively, which are observed during the stance phase, from around 10 to 50% of the gait cycle.

B.3 Conclusion

A deviation of the perpendicular distance d from the segment axis to the posterior side of the segment or the distance h from the knee joint axis to the attachment of the cylinder, parallel to the segment axis, influences the knee joint angle, the desired torque, and the desired force calculated by the force control mechanism. Therefore, an incorrect amount of force could be delivered by the orthosis if it is not attached to the body according to the guidelines.
The influence of a wrong assumption for the distance h on the knee joint angle, the desired torque, and the desired force is larger compared to the influence of a wrong assumption for the distance d. Therefore, a deviation in the distance h will have a larger effect of the force delivered by the orthosis compared to a deviation in the distance d.
Since the effect of a deviation of the distances d and h in the same direction has an opposite effect on the desired force, it could be possible that the effect of the deviations of the distances cancels out. Therefore, the desired force may have the expected magnitude, despite those deviations of the distances in opposite directions.

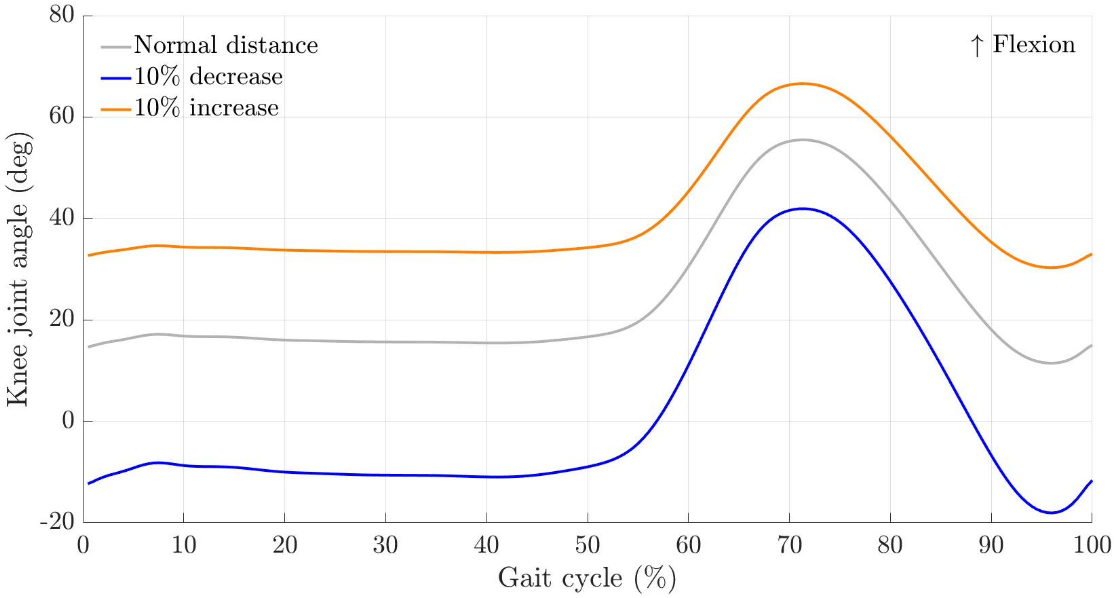

Figure B.2: The knee joint angle during minimal impedance mode trials, averaged across all subjects, and the simulated knee joint angle for a 10% decrease and increase of the distance h from the knee joint axis to the attachment of the cylinder, parallel to the segment axis.

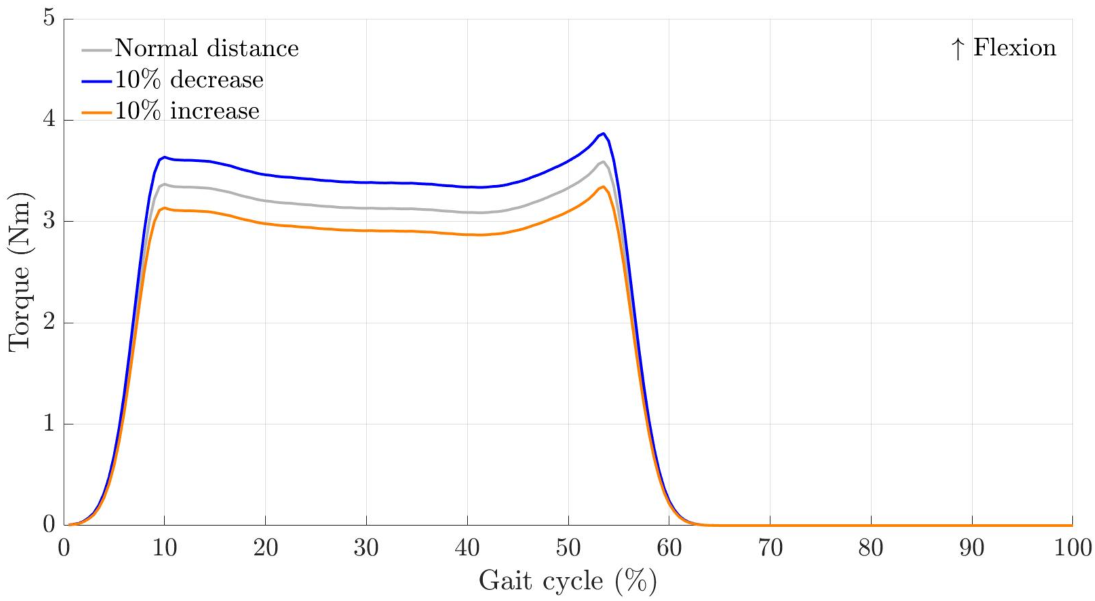

Figure B.3: The desired torque during minimal impedance mode trials, averaged for one subject, and the simulated desired torque for a 10% decrease and increase of the perpendicular distance d from the segment axis to the posterior side of the segment.

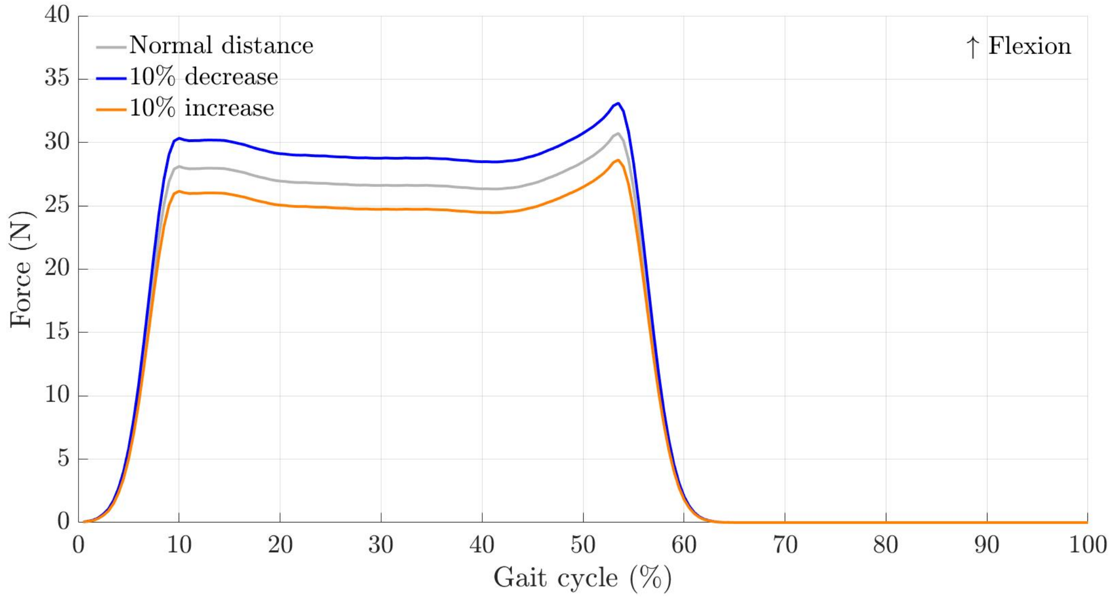

Figure B.4: The desired force during minimal impedance mode trials, averaged for one subject, and the simulated desired force for a 10% decrease and increase of the perpendicular distance d from the segment axis to the posterior side of the segment.

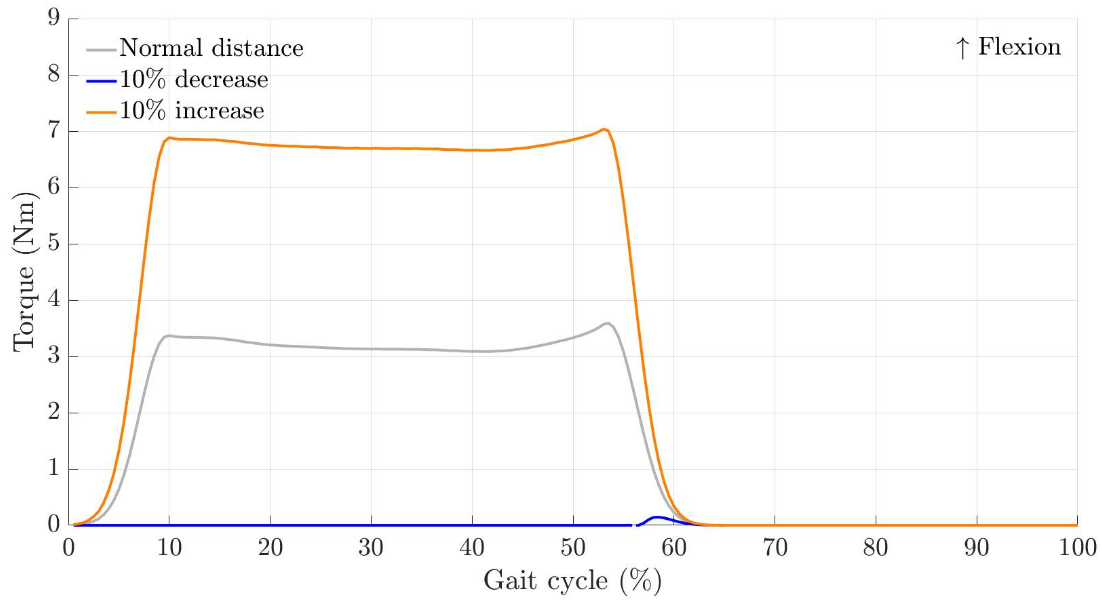

Figure B.5: The desired torque during minimal impedance mode trials, averaged for one subject, and the simulated desired torque for a 10% decrease and increase of the distance h from the knee joint axis to the attachment of the cylinder, parallel to the segment axis.

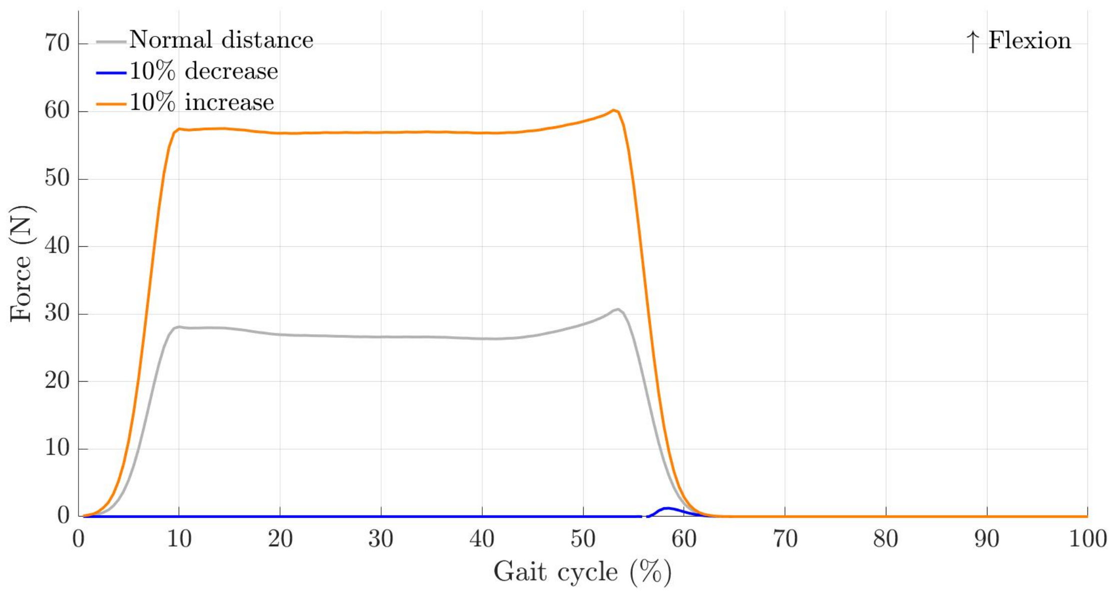

Figure B.6: The desired force during minimal impedance mode trials, averaged for one subject, and the simulated desired force for a 10% decrease and increase of the distance h from the knee joint axis to the attachment of the cylinder, parallel to the segment axis.